Enhanced functionality of low-affinity CD19 CAR T-cells is associated with activation priming and a polyfunctional cytokine phenotype

Ilaria M. Michelozzi[1], Eduardo Gomez Castaneda[1*], Ruben V.C. Pohle[1*], Ferran Cardoso Rodriguez[2], Jahangir Sufi[2], Pau Puigdevall Costa[3], Meera Subramaniyam[1], Efstratios Kirtsios[1], Ayad Eddaoudi[1], Si Wei Wu[1], Aleks Guvenel[1], Jonathan Fisher[4], Sara Ghorashian[5], Martin A. Pule[6], Christopher J. Tape[2], Sergi Castellano[3,7#], Persis J. Amrolia[1,5#] and Alice Giustacchini[1].

1. Molecular and Cellular Immunology Section, UCL Great Ormond Street Institute of Child Health, London, UK

2. Cell Communication Lab, Department of Oncology, University College London Cancer Institute, London, UK

3. Genetics and Genomic Medicine Department, Great Ormond Street Institute of Child Health, University College London, London, UK

4. Developmental Biology and Cancer Section, UCL Great Ormond Street Institute of Child Health, London, UK

5. Department of Bone Marrow Transplant, Great Ormond Street Hospital for Children, London, UK

6. Cancer Institute, University College London, London, UK

7. UCL Genomics, Great Ormond Street Institute of Child Health, University College London, London, UK

*These authors (E.G.C and R.V.C.P.) contributed equally to this work

#These authors (S.C. and P.J.A.) contributed equally to this work

Corresponding author: Alice Giustacchini (a.giustacchini@ucl.ac.uk)

Abstract

We recently described a low-affinity second-generation CD19 chimeric antigen receptor (CAR) CAT that showed enhanced expansion, cytotoxicity, and anti-tumour efficacy compared to the high-affinity (FMC63 based) CAR used in Tisagenlecleucel, in pre-clinical models. Furthermore, CAT demonstrated an excellent toxicity profile, enhanced *in vivo* expansion, and long-term persistence in a Phase I clinical

study. To understand the molecular mechanisms behind these properties of CAT CAR T-cells, we performed a systematic *in vitro* characterization of the transcriptomic (RNA-seq) and protein (CyTOF) changes occurring in T-cells expressing low-affinity *vs* high-affinity CD19 CARs following stimulation with CD19-expressing cells. Our results show that CAT CAR T-cells exhibit enhanced activation to CD19 stimulation and a distinct transcriptomic and protein profile, with increased activation and cytokine polyfunctionality compared to FMC63 CAR T-cells. We demonstrate that the enhanced functionality of low-affinity CAT CAR T-cells is a consequence of an antigen-dependent priming induced by residual CD19-expressing B-cells present in the manufacture.

Research Article

Introduction

T-cells genetically engineered to express CD19 chimeric antigen receptors (CAR T-cells) have shown remarkable efficacy in relapsed/refractory (r/r) B-cell malignancies leading to clinical licensing for r/r B-cell acute lymphoblastic leukaemia (B-ALL) and Non-Hodgkin Lymphoma[1]. Despite this success, several safety and efficacy hurdles remain[2]. CAR T-cells can trigger potent immune responses leading to transient but potentially life-threatening inflammatory events, such as cytokine release syndrome (CRS) and neurotoxicity[3,4]. CAR T-cell engraftment and expansion is a prerequisite for efficacy. Not all CD19 CAR T-cell products persist *in vivo* and long-term immune surveillance appears critical for preventing disease relapse, particularly in ALL. Thus, the design of versatile CAR T-cells, capable of balancing safety and efficacy, is contingent on our understanding of the molecular mechanisms underlying CAR T-cell function. The engagement of CARs to their cognate antigens results in the activation of CAR T-cells and promotes their rapid expansion as well as their differentiation into distinct T-cell subsets, mediating tumour cytolysis (effector cells) and providing long-lasting protection (memory cells). As tumour cell recognition by CAR T-cells relies on the binding of the CAR's single-chain variable fragment (scFv) to its epitope, fine-tuning the affinity of CARs to their antigens has become a strategy to modulate the strength of CAR T-cell responses[5].

The affinity of CARs is determined by their binding kinetics and the rates at which they associate to and dissociate from their targets. The optimal affinity of a CAR is likely to vary depending on a number of factors, including the CAR design, the CAR expression levels and the antigen density on the target cells[6,7]. Chimeric immunoreceptors have an activation ceiling above which increasing the binding affinity does not improve T-cell activation but can rather result in T-cell exhaustion[8]. In contrast, by reducing CAR scFv affinity, the strength of the T-cell signal can be modulated, so that CAR T-cells

discriminate different levels of antigen expression. CARs exhibiting slower antigen-association rates to ErbB2, EGFR and CD123 targets showed reduced activation in response to low antigen concentrations, favouring differential targeting of tumour cells overexpressing the target *vs* normal tissue expressing the same target at physiological levels[8-10]. We have recently described a novel low-affinity CD19 CAR (CAT), with epitope, structure and stability similar to the widely used FMC63, but characterized by faster rates of antigen dissociation, leading to an overall 40-fold reduction of its affinity[11]. Pre-clinical testing of CAT CAR T-cells has revealed greater antigen-specific cytotoxicity, higher proliferation both *in vitro* and *in vivo* and more potent *in vivo* anti-tumour activity when compared to FMC63. In a Phase I clinical trial in patients with high-risk treatment-refractory paediatric B-ALL, CAT CAR T-cells resulted in lower toxicity in terms of severe CRS and displayed greater expansion than that reported for the FMC63 based tisagenlecleucel as well as excellent persistence[11]. These results were recently confirmed in a multicenter Phase I trial in r/r adult B-ALL[12].

In this regard, while CAT CAR T-cells have been designed to explore the possibility to prevent excessive activation and reduce CRS and neurotoxicity risks, enhancements in their cytotoxicity, expansion and persistence were unexpected[7] and the underlying molecular mechanisms to these functional phenotypes remain unknown.

The molecular mechanisms through which the fine-tuning of CARs affinity influences CAR T-cell phenotypes and functions are largely unknown. The interaction between T-cell receptor (TCR) and the peptide-MHC complex offers however some insight on how immunoreceptors' affinity can dramatically influence T-cell functions[13]. Faster target off-rates in TCRs allow a single peptide-MHC complex to serially trigger several TCRs, resulting in amplified and sustained T-cell activation[13]. Similar to TCRs, low-affinity CARs may lead to enhanced T-cell activation and decreased exhaustion.

Herein we perform a systematic *in vitro* characterization of the molecular and biochemical changes occurring in CAR T-cells, comparing a low-affinity CD19 CAR (CAT) with a high-affinity one (FMC63). By combining bulk RNA sequencing with single-cell mass cytometry analyses (cytometry by time of flight, CyTOF), we show that the expression of the CAT CAR induces an antigen-dependent priming in response to low concentrations of CD19-expressing B-cells found in the manufacture product. Upon antigen stimulation, we identified distinct molecular features downstream of CAT CAR activation responsible for enhancing CAT CAR T-cell functional response.

Results

Generation and quality assessments of low- (CAT) and high- (FMC63) affinity CD19 CARs from healthy donors

To dissect the molecular mechanisms behind the functional differences observed between low- (CAT) and high- (FMC63) affinity CD19 CAR T-cells[11], we interrogated the transcriptional and protein expression profiles of T-cells lentivirally (LV) transduced with CARs differing only in their scFv (Supplementary Fig. 1a). We performed bulk transcriptomic analyses (RNA-seq) to identify CAR T-cell distinct gene expression signatures and mass cytometry analyses (CyTOF) to model differences in their downstream signalling at a single-cell resolution[14]. RNA-seq and CyTOF readouts from untransduced (UNTR) controls and T-cells LV transduced to express CAT or FMC63 CD19 CARs from healthy donors (HD1-HD27, Supplementary Table 1) were compared at baseline and following stimulation with CD19+ ALL cell line NALM6 (unstimulated and stimulated conditions, respectively), as schematized in Fig. 1a. Importantly, we ruled out significant differences in the transduction of the two CARs by fluorescence activated cell sorting (FACS), assessing the percentage of mCherry+ T-cells (LV fluorescent reporter) across donors and experimental conditions. These ranged between 11.50 - 93.80% (median 39.1%) in FMC63 and 13.40 - 93.60% (median 36.25%) in CAT (Fig. 1b, left) and were thus comparable among individual HDs. In agreement, we found similar transgene expression levels between the 2 CARs by measuring mCherry mean fluorescent intensity (MFI), a proxy for CARs expression (Fig. 1b, right) and by quantifying CARs surface expression levels (Fig. 1c) and number of integrated vector copies (VCN) (Supplementary Fig. 1b). Finally, we assessed CAT and FMC63 CAR T-cell products for their CD4:CD8 ratios and memory T-cell subsets composition, as these characteristics can both affect CAR T-cells persistence and anti-tumour activity[15,16]. While no difference in CD4:CD8 ratios was observed in the absence of antigen stimulation (Fig. 1d), the proportion of memory subsets differed in unstimulated FMC63 and CAT CAR T-cells, as measured by FACS at 10 days post-transduction. CAT CAR T-cells exhibited a significant increase in the fraction of central memory T-cells (T_{CM}, CD62+CD45RA-) as compared to both UNTR and FMC63 conditions (Fig. 1e, left). The increase in T_{CM} was largely at the expense of T effector memory cells (T_{EM}, CD62-CD45RA-) and effector memory re-expressing CD45RA (T_{EMRA}, CD62-CD45RA+), whose proportion was significantly reduced in CAT *vs* FMC63 CAR T-cells and in both CARs as compared to UNTR control (Fig. 1e, middle and right). These assessments confirmed that our CAR T-cell products were suitable to investigate the molecular features of CAT and FMC63 CAR T-cells.

Low-affinity CD19 CAT CARs display higher activation priming during CAR T cell manufacture

134 We next performed bulk RNA-seq of FACS-sorted UNTR T-cells (CD3+) and FMC63 or CAT CAR T-cells
135 (CD3+mCherry+) expanded for 4 days with or without stimulation with NALM6 at 24 h post-
136 stimulation. Transcriptomics confirmed that mCherry was an accurate proxy for CAR transgene
137 expression levels, as evidenced by the significant positive correlation between the MFI of mCherry by
138 FACS and the normalized RNA-seq counts aligning to the scFv region of each of the 2 CARs
139 (Supplementary Fig. 2a). Similarly, the proportion of CD4 and CD8 T-cells detected by FACS was in line
140 with the *CD4* and *CD8* mRNA levels (Supplementary Fig. 2b, c). Principal component analysis (PCA) on
141 the 500 most variable expressed genes (top 100 genes shown in Supplementary Fig. 2d), distributed
142 samples according to a T-cell activation gradient (PC1, from UNTR to CAR activated samples) (Fig. 2a).
143 The majority of variance in gene expression across experimental conditions was explained by CD19-
144 mediated CAR activation. As expected, UNTR T-cells not expressing any CARs were largely unaffected
145 by antigen stimulation (Fig. 2a). Similarly, PCA on protein expression from CyTOF, based on earth
146 mover's distance (EMD) scores (a sensitive measure of multivariate changes in protein levels)[17], in the
147 same experimental conditions and timepoints than the gene expression, followed a similar gradient
148 of sample activation, shifting from UNTR samples to antigen stimulated CAR T-cells on PC1 (Fig. 2b
149 and Supplementary Fig. 3a). The most variable genes upregulated upon stimulation with NALM6 in
150 both FMC63 and CAT CAR T-cells included genes involved in T-cell activation (*IL2RA*, *GZMB*) and
151 proliferation (*PCNA*, *LDHA*), which are expressed at very low levels in control T-cells (Supplementary
152 Fig. 2d). Consistent with this, the highest protein expression variation was from markers of T-cell
153 activation (CD25, NFAT1, HLA-DR) and proliferation (pRB) (Supplementary Fig. 3a). Of note, both RNA
154 and protein analyses unstimulated CAR T-cells had an intermediate RNA/protein expression profile
155 between UNTR and stimulated CAR T-cells. This suggests that CAR expression on its own, in absence
156 of antigen stimulation, induces basal T-cell activation (Fig. 2a-b). Importantly, unstimulated CAT
157 samples appear closer to antigen stimulated CAR T-cells than unstimulated FMC63, as well as having
158 less overlap with UNTR samples suggesting unstimulated CAT CAR T-cells show a degree of pre-
159 activation even prior to antigen stimulation.
160
161 To gain further insights into the intermediate activation state observed in unstimulated CAT, we fuzzy
162 clustered genes by their gene expression and classified individual samples into more than one cluster
163 to resolve intermediate cell states and trajectories (Fig. 2c)[18]. We identified two clusters, highly
164 enriched for either inactive T-cells (cluster 1, which includes UNTR samples) or antigen-activated CAR
165 T-cells (cluster 2, which includes stimulated CAR T samples) (Fig. 2c). Notably, the probability of
166 unstimulated CAT samples of belonging to cluster 2 (activated CAR T-cells) was substantially higher
167 than that of unstimulated FMC63 (4/6 HDs in CAT *vs* 0/6 HDs inFMC63), further evidencing the

168 functional proximity between unstimulated CAT and activated CAR T-cells. In this regard, using gene
169 set enrichment analyses (GSEA) on the Hallmark collection, we confirmed that while antigen
170 stimulated CAT and FMC63 CAR T-cells have similar enrichment for most of the gene sets involved in
171 immune functions and cell proliferation, in the absence of antigen stimulation CAT CAR T-cells are
172 uniquely enriched for T-cell activation pathways (Myc Targets V1, Hedghog signalling, Inflammatory
173 response, Interferon α response) (Supplementary Fig. 3b).
174 To investigate whether the introduction of high- or low-affinity CD19 CARs can differentially affect
175 gene expression patterns in T-cells, we directly compared the transcriptome of FMC63 and CAT CAR
176 T-cells, in absence of antigen stimulation. Following differential gene expression (DGE) analysis, we
177 found that only 10 genes were significantly DE between these two conditions (FDR < 0.1,
178 Supplementary Table 2), 9 of which were upregulated in CAT *vs* FMC63 CAR T-cells. Among those, we
179 found genes involved in cytotoxicity (*GNLY*, *GZMK*) and markers of T-cell activation such as MHC class
180 II molecules (MHCII) (*HLA-DRA* and *HLA-DPA*) (Fig. 2d). This supports our previous observation of gene
181 expression in unstimulated CAT resembling more that of antigen activated CAR T-cells than gene
182 expression in unstimulated FMC63 (Fig. 2c). Mass cytometry analyses using a panel of antibodies
183 against markers of T-cell activation (Supplementary Table 3), confirmed that while unstimulated
184 FMC63 and CAT CAR T-cells have similar EMD scores for many of the proteins investigated
185 (Supplementary Table 5a), unstimulated CAT CAR T-cells have significantly stronger activation priming
186 with higher expression of markers of T-cell activation (HLA-DR, CD25 and NFAT1), pro-inflammatory
187 (Granzyme B, Perforin B) and stimulatory/activation-related (GM-CSF, IL-17A) cytokines and increased
188 phosphorylation of the TCR/CAR CD3ζ chain (pZAP70) and MTOR downstream effector (pS6) (Fig.2e
189 and Supplementary Fig. 3c).
190 Altogether, these results show that unstimulated CAT CAR T-cells, prior to antigenic stimulation, have
191 more pronounced T-cell activation priming than FMC63 CAR T-cells.
192
193 **CD19 stimulation of low-affinity CAT CAR T-cells results in a distinct transcriptomic and protein**
194 **profile with increased activation/proliferation over high-affinity FMC63 CAR T-cells**

195 While antigen-independent CAR activation, also known as tonic signalling, has been historically
196 associated with CAR T-cell accelerated differentiation and exhaustion[19-21], recent data show that the
197 induction of CAR T-cell priming, by either 4-1BB-based tonic signaling[22] or by low-dose
198 hypomethylating agents[23], can lead to CAR T enhanced anti-tumour functions *in vivo*. In light of these
199 observations, we next wanted to assess the molecular impact of the "activation priming" observed in
200 CAT CAR T-cells on their molecular response to antigen stimulation. As the superior cytotoxicity of CAT
201 CAR T-cells over FMC63 CAR T-cells has been previously shown in functional assays[11], we focused on

202 characterizing their distinct molecular profiles upon exposure to antigenic stimulation. Upon
203 stimulation, we found a slight but statistically significant reduction of CD4:CD8 ratio in CAT as
204 compared to FMC63 (Fig. 3a). This variation was largely attributable to a relative decrease of the CD8+
205 fraction (and increase of CD4+) in FMC63 CAR T-cells after antigen stimulation (Supplementary Fig.
206 4a). Interestingly, when looking at the memory T-cell subsets composition after antigenic stimulation,
207 we found that CAT CAR T-cells continued to exhibit a higher proportion of T_{CM} as compared to FMC63
208 (Fig. 3b), while no differences were observed in the expression of exhaustion markers (PD1, TIM3 and
209 LAG3) between the two CAR constructs (Fig. 3c).

210 Importantly, the stronger basal activation observed in CAT CAR T-cells did not prevent an even
211 stronger molecular response when exposed to CD19-expressing NALM6, as shown by the increase in
212 the expression of proliferation and cytotoxic/stimulatory markers, relatively to the unstimulated
213 constructs (Supplementary Fig. 5 and 6). Consistent with this, after stimulation with NALM6, we
214 identified 51 DE genes, 35 of which were upregulated in CAT compared to FMC63 (Fig. 3d and
215 Supplementary Table 4). CD19 stimulation in CAT CAR T-cells also led to significantly augmented
216 expression of immune stimulatory/proliferation cytokines (*IFNG, CSF2, CXCL8*), and IFN-γ responsive
217 genes (*CIITA*) (Fig. 3d and Supplementary Fig. 4b). Conversely, CAT CAR T-cells displayed significantly
218 decreased expression of the genes encoding for CRIF1 (*GADD45GIP1*), an inhibitor of cell cycle
219 progression, and for FOXP3, the Treg-associated transcription factor known to be only transiently
220 expressed in the initial stages of Th1 response and rapidly downregulated afterwards[24,25] (Fig. 3d).
221 These results suggest that following antigenic stimulation CAT CAR T-cells show a different
222 transcriptomic profile resulting in stronger activation and proliferation than stimulated FMC63. In
223 addition, CAT CAR T-cells showed increased expression of the *TNFSF4* gene (Fig. 3d), encoding for the
224 ligand of the T-cell co-stimulatory receptor OX40 (OX40L). While OX40L is mainly expressed by antigen
225 presenting cells to promote T-cell activation during antigenic stimulation, it is also expressed in
226 activating T-cells, where it leads to a homotypic OX40L-OX40 signalling axis promoting T-cell longevity
227 and memory differentiation[26]. Further, we also noted the increased expression of the
228 chemoattractants *CCL4* and *CCL3L1* and genes involved in cell migration (*FLT1*, *DOCK5*) and focal
229 adhesion (*COL6A3*) in stimulated CAT CAR T-cells (Supplementary Fig. 4b). Importantly, the secretion
230 of CCL4 and CCL3 by activated T-cells has been shown to mediate T-cell attraction toward one another,
231 promoting T-cell clusters formation and synaptic cytokines exchange coordinating immune
232 responses[27-30]. Single cell transcriptomic studies have recently revealed that subsets of CAR T with
233 elevated expression of CCL3 and CCL4 are associated to longer persistence *in vivo*[31] and achievement
234 of complete remission[32].

235 These observations were further substantiated at the protein level. Indeed, CAT CAR T-cells exhibited
236 a marked increase in the expression (as measured by EMD score) of markers of T cell activation (CD25)
237 (Fig. 3e). Moreover, the augmented gene expression of the MHCII trans-activator CIITA observed in
238 CAT, resulted in a corresponding increase of HLA-DR protein (Fig. 3e)[33,34]. When measuring the CAR T-
239 cell intracellular signalling, CAT CAR T-cells showed enhanced phosphorylation of the effectors of the
240 TCR/CAR CD3ζ chain (pZAP70, pp38) and increased expression of their downstream transcription
241 factors (NFAT1, pCREB, FOXP3). CAT CAR T-cells also exhibited significant upregulation of the Target
242 of Rapamycin Complex 1 (mTORC1) downstream effectors (pS6 and pRB), both involved in cell
243 proliferation and protein translation, in line with the previously reported CAT CAR T cells increased
244 proliferative capacity over FMC63[11].

245 Our analysis shows that the increased "activation priming" observed in CAT CAR T-cells over FMC63
246 resulted in an even stronger T-cell activation gene expression and signaling profile when CAT CAR T-
247 cells were exposed to antigenic stimulation. These observations are in line with the CAT CAR T cells
248 enhanced cytotoxic functional properties previously reported[11].

249 **The enhanced functionality of low-affinity CD19 CAR T-cells is associated with cytokine**
250 **polyfunctionality upon antigen stimulation**
251
252 We next assessed CAR T-cell functional phenotypes by measuring intracellular cytokines levels in
253 individual cells by mass cytometry. The overall protein intensities measured by EMD scores indicated
254 an increased expression of effector cytokines (Granzyme B , IFN-γ and TNF-α) and of immune
255 stimulatory molecules (GM-CSF and IL-2) in CAT CAR T as compared to FMC63 (Figure 4a). No
256 upregulation was observed for Th2/immune-modulatory cytokines (IL-4, IL-5 and TGF-ß) and for
257 Perforin B (Supplementary Table 5b).
258
259 Next, we investigated the overall pattern of cytokine co-expression in CAT and FMC63 CAR T-cell
260 responses. The ability of a single T-cell to express simultaneously more than one cytokine
261 (polyfunctionality) has been linked to productive immune responses[35,36] and more recently described
262 as a distinctive feature of CAR T-cells associated to their potency and anti-tumour efficacy [37-39]. We
263 measured the frequency at which the eight cytokines included in our analysis were co-expressed in
264 single CAR T-cells, thus providing a comprehensive profile of their cytokine polyfunctionality. Upon
265 stimulation with NALM6, 15.02% of FMC63 and 29.60% of CAT CAR T-cells were polyfunctional
266 (expressing two or more cytokines per cell) (Supplementary Table 5n).

267 Furthermore, not only the frequency of polyfunctional CAR T-cells, but also the number of cytokines
268 co-expressed was higher in CAT than in FMC63, with a stastically significant increase in their mean
269 polyfunctionality (Fig. 4b) and a marked increment in the proportion of cells expressing combinations
270 of three or more cytokines (2.28% in FMC63 *vs* 7.89% in CAT) (Fig. 4c and Supplementary Table 5o).
271 The polyfunctional profiles of stimulated CAT CAR T-cell products were dominated by combinations
272 of cytokines involving the effector molecules IFN-g, TNF-α, IL-2 and Granzyme B (Fig. 4d).

273 **Low-affinity CD19 CAT CAR activation priming is associated with and driven by residual CD19-**
274 **expressing B-cells**

275 To investigate whether the mechanism behind the activation priming observed in unstimulated CAT
276 CAR T-cells was antigen-dependent or -independent, we checked if residual CD19+ B-lymphocytes
277 were detectable in the CAR T-cell product and could serve as a potential source of antigen specific
278 activation.
279
280 We monitored the proportion of CD19+ B-lymphocytes in culture at different timepoints. While B-cells
281 were detectable at day 0 in all samples (5.96% of cells on average), at day 8 (5 day stimulation with
282 CD3/CD28 beads + 3 day rest) they could only be detected in the UNTR condition (2.33% of cells on
283 average), and had been completely depleted from both CAR constructs, as shown by FlowSOM
284 analysis of mass cytometry data, clustering single-cells by cell types[40], and the relative frequencies
285 (Fig. 5a and Supplementary Fig. 7a). To test whether the activation priming observed in CAT CAR T-
286 cells was dependent on donor B-cells, we applied the experimental setup described in Fig. 1a, only
287 now including as additional experimental condition CAR T-cells generated from CD19-depleted
288 PBMCs. We confirmed effective CD19 depletion by flow cytometry, with an average of residual B cells
289 of 0.041% upon depletion as compared to 5.96% with the standard protocol (Supplementary Fig. 7b).
290 The transduction levels obtained in the CD19-depleted CAT and FMC63 CAR T-cells were comparable
291 based on the expression of the fluorescent reporter (mCherry) and the VCN (Supplementary Fig. 7c-
292 d). The baseline CD4:CD8 ratios only showed a slight increase in CAT as compared to FMC63 CAR T
293 cells (Supplementary Fig. 7e). Of note, CD19-depletion impacted on the T memory subsets
294 composition, with CAT CAR T-cells no longer displaying any statistical difference when compared to
295 the UNTR control, while FMC63 CAR T-cells still showing a significant increase in the proportion of T_{EM}
296 when compared to the UNTR control (Fig.5b).
297 Mass cytometry analyses revealed that the residual B cells in the CAR T-cell manufacture were
298 responsible for the activation priming observed in unstimulated CAT and FMC63 CAR T-cells
299 (Supplementary Fig. 8, 9). While CD19 depletion led to a general decrease in the activation priming

300 previously observed in unstimulated CAR T-cells, this reduction was more pronounced in CAT
301 (Supplementary Fig. 8) than in FMC63 (Supplementary Fig. 9). As a result, upon B cell depletion we no
302 longer detected statistically significant differences in the expression of T-cell activation markers (HLA-
303 DR, CD25 and NFAT1), pro-inflammatory cytokines (Granzyme B, Perforin B) and CAR-downstream
304 signaling molecules (pZAP70 and pS6) between CAT and FMC63 (Fig.5c). Differential protein
305 expression between CD19-depleted CAT and FMC63 CAR T-cells was only observed for pRB and CD69
306 (Supplementary Fig. 7f). Both CAT and FMC63 CAR T cells exhibited increased expression of activation
307 and cytotoxic markers with respect to the UNTR controls they are normalized to, indicating similar
308 levels of antigen-independent activation (Fig. 5c).
309 When later exposed to CD19-expressing NALM6, both CD19-depleted CAT and FMC63 were able to
310 activate, as shown by the upregulation of the expression of cytotoxic markers and cytokines compared
311 to their unstimulated counterparts (Supplementary Fig. 10, 11). No differences in the CD4:CD8 ratios
312 and in the expression of exhaustion markers were observed between the two stimulated CAR
313 conditions upon CD19-depletion (Supplementary Fig. 7g, h). Most importantly, upon antigenic
314 stimulation, CD19-depleted CAT CAR T-cells activated a molecular response with no stastically
315 significant differences when compared to FMC63 (Fig. 5d and Supplementary Fig.7i), except for an
316 increased expression of IL-2 (Supplementary Fig.7i). In agreement, the increased cytokine
317 polyfunctionality observed in CAT *vs* FMC63 CAR T-cells in standard manufacture condition (Fig. 4) was
318 no longer observed in CD19-depleted manufacture condition (Fig. 5e).
319
320 Altogether these results demonstrate that residual B-cells in the CAR T-cell manufacture can mediate
321 an antigen dependent activation priming, which is more pronounced in low affinity CAT CAR T-cells
322 when compared to FMC63 CAR T-cells. Such activation priming contributes to boosting CAT CAR T-cell
323 response, as CAT CAR T-cells generated from CD19-depleted PBMCs not only do not display increased
324 activation priming but also do not exhibit increased molecular responsed to antigenic stimulation with
325 NALM6.

326 **Discussion**

327
328 Modulating CAR T-cell affinity may enable us to enhance anti-tumour response and long-term tumour
329 surveillance, while minimizing CAR T-cell related toxicity. To this aim, characterizing the molecular
330 determinants of treatment efficacy in the low-affinity CAT CAR may inform future design and optimize
331 their manufacture. We thus investigated the transcriptomic and proteomic phenotype of CD19 CAT
332 CAR T-cells, compared with the widely used FMC63, to begin unravelling the molecular mechanisms
333 behind the observed preclinical and clinical differences between these two CD19 CARs[11].

334 We found that CAT CARs induce stronger activation responses than FMC63, which could be explained
335 by the faster target off-rate of low-affinity CARs. Faster dissociation requires fewer targets to serially
336 trigger a larger number of CARs and amplify anti-tumoural response[13]. This would align with the
337 proposed model of temporal and spatial summation of T-cell activation, in which signals from serially
338 triggered immunoreceptors can be accumulated and integrated overtime to reach the threshold
339 required for T-cell activation[41]. This model may also explain why low levels of residual donor B cells in
340 the manufacture can induce stronger activation priming in CAT CAR T cells than in FMC63. However,
341 as CAT and FMC63 have been predicted to bind overlapping but not necessarily identical epitopes on
342 CD19, we cannot exclude that the epitope location could also contribute, in part, to the functional
343 differences observed[11,42].
344 Our transcriptomic and protein profiling revealed that unstimulated CAT CAR T-cells are functionally
345 closer to antigen activated CAR T-cells than FMC63 CAR T-cells, with a number of upregulated
346 activation genes (*HLA-DBP1*, *HLA-DRA* etc) and proteins (HLA-DR, CD25 and NFAT1). Despite these
347 genes/proteins being commonly associated to T-cell activation, their basal expression is also increased
348 in memory T-cells as compared to $T_{NAÏVE}$ cells. This is because memory T-cells are characterized by an
349 open chromatin conformation favouring the access of transcription factors to immune response
350 genes, thus ensuring a pool of readily available mRNAs that can be rapidly translated following
351 stimulation[43]. This hypothesis would be in agreement with the increased proportion of T_{CM} observed
352 in CAT CAR T cells as compared to FMC63.
353
354 By performing B cell depletion prior to CAR T-cell manufacture, we demonstrate that residual B-cells
355 expressing CD19 in the CAR T-cell product are responsible for the activation priming observed in CAR
356 T-cells, which was more pronounced in CAT when compared to FMC63. This is consistent with the
357 hypothesis that CAT serial triggering may amplify T-cell activation from lower antigen levels[13] and
358 points to a boosting role of low dose CD19-priming during CAR T-cell manufacture. Recent results have
359 shown that antigen-independent induction of CAR T-cell priming, by either 4-1BB-based tonic
360 signalling[22] or by low-dose of hypomethylating agents[23] can lead to enhanced CAR T anti-tumour
361 functions *in vivo*. Our results indicate that low dose antigen-specific priming can also promote CAR T-
362 cell functionality in a CAR construct specific manner with an enhanced effect in low-affinity CAR T-
363 cells. This results may appear controversial, relatively to the increasing evidence that CD4/CD8 T-cell
364 positive selection prior to manufacture leads to CAR T-cell products outperforming those derived from
365 unfractionated leukaphereses. However, the improved performance of CD4/CD8 CAR T cell
366 manufactures has been mechanistically linked to the depletion of myeloid and NK cells negatively

367 impacting CAR T cell transduction, activation and expansion, while the role of B cells has not been
368 extensively investigated in this setting[44-46].
369

370 When stimulated with CD19-expressing NALM6 cell line, CAT CAR T-cells have a distinct transcriptomic
371 and protein response to CD19 antigenic stimulation from FMC63 CAR T-cells with increased expression
372 of proliferation, activation and cytotoxic markers at both RNA and protein levels. *In vivo* clonal kinetics
373 analyses have shown that single CD19 CAR T-cells with higher expression of cytotoxic related genes in
374 the manufacture product, many of which in common with ours (including *IFNG*, *HLA-DRA*, *CCL4*), gave
375 rise to superior *in vivo* expansion and survival, significantly contributing to later timepoints after
376 adoptive transfer in patients[19,31]. Analysis of gene expression also revealed the upregulation of
377 chemoattractive cytokines CCL4 and CCL3L1 in CAT, which induce T-cell homotypic interactions and
378 promote the reciprocal exchange of self-reinforcing signals such as OX40L,[26,29] which are upregulated
379 in CAT as well. Single-cell transcriptomic studies have recently revealed that subsets of CAR T with
380 elevated expression of CCL3 and CCL4 are associated to longer persistence in vivo[31] and achievement
381 of complete remission[32]. Mass Cytometry analyses revealed a CAT CAR T enhanced activation protein
382 profile, as measured by the increased expression of T-cell activation markers (CD25, HLA-DR) and CAR
383 downstream signaling effectors (pZAP70, pp38, NFAT1, pCREB, FOXP3). Furthermore, CAT CAR T-cells
384 showed increased mTORC signaling (pS6 and pRB), which is commonly associated to cell proliferation
385 and protein translation. Altogether, CAT CAR T-cells distinct gene expression and protein profiles are
386 very much in line and likely responsible for the enhanced proliferative responses that CAT CAR T-cells
387 exhibited *in vitro*, in *in vivo* murine models and in patients, as previously reported by Ghorashian et
388 al.[11].

389

390 Upon stimulation, CAT CAR T-cells were also characterized by a unique polyfunctional pattern of
391 cytokine expression, with a marked increase in the frequency of single CAR T-cells expressing >=3
392 cytokines when compared to FMC63. CAT polyfunctional profile was dominated by combinations of
393 effector cytokines, consistent with their potent anti-tumour activity. It has been suggested that the
394 ability of CAR T-cells to produce multiple cytokines (polyfunctionality) in response to antigen exposure
395 is associated with improved anti-tumour responses *in vivo*[37] and cytokine polyfunctionality has been
396 recently proposed as a criteria to predict CAR T-cell potency [39]. The increased cytokine
397 polyfunctionality observed in CAT CAR T-cells contributes to explain their increased cytotoxic potential
398 previously observed *in vitro settings* and in *in vivo* murine models[11].
399

400 In conclusion, we describe the molecular mechanisms underlying the low-affinity CAT CAR T-cell
401 functional phenotype. We provide evidence that the potent and long-term anti-tumour responses
402 observed with low-affinity CAT CAR T-cells[11] reflect a distinct pattern of both activation priming and
403 cytokine polyfunctionality. We show that low affinity CAT CAR T-cells are preferentially primed by low
404 concentration of CD19-expressing B-cells present in the manufacture and such priming is instrumental
405 to their higher cytotoxic response upon stimulation. Although our observations are limited to one low-
406 affinity CAR, future work extending this characterization to a panel of low-affinity CARs, may reveal at
407 which extent these findings are generalisable. Overall, our work has important implications for the
408 future design of versatile CAR T-cells manufacture protocols, capable of boosting efficacy and long-
409 term persistence.
410

411 **Methods**

412

413 **Human peripheral blood samples and cell lines**

414

415 Peripheral blood was collected from 20 HDs after having obtained informed consent. Fresh
416 mononuclear cells were isolated by Ficoll density gradient centrifugation (day 0) and used for
417 experiments (standard condition). CD19+ B cells were magnetically removed from freshly isolated
418 PBMCs using CD19 Microbeads (Miltenyi Biotec, Bergisch Gladbach, Germany) according to
419 manufacturer's recommendations (depleted condition). All analyses were performed on fresh T- or
420 CAR T-cells except for one 96 h memory subset FACS analysis. HD details and relative experimental
421 procedure are reported in Supplementary Table 1. The human ALL cell line NALM6 was purchased
422 from DSMZ. Cells were cultured according to manufacturer's instructions in complete RPMI 1640
423 medium, GlutaMAX™ Supplement (Gibco™, Thermo Fisher Scientific, Waltham, MA, USA)
424 supplemented with 10% of heat-inactivated Foetal Bovine Serum (FBS) (Gibco™, Thermo Fisher
425 Scientific), 100 IU penicillin and 100 μg/ml streptomycin (Sigma-Aldrich, St. Louis, MO, USA).
426

427 ***Ex vivo* T-cell expansion**

428

429 Freshly isolated PBMCs and CD19-depleted PBMCs were cultured in TexMACS™ medium (Miltenyi
430 Biotec, Bergisch Gladbach, Germany), an optimised T-cell medium. To induce T-cell expansion,
431 CD3/CD28 beads (CTS™ Dynabeads™ CD3/CD28, Thermo Fisher Scientific) were added to cells in
432 MACS GMP Cell Differentiation Bags (Miltenyi Biotec) at a 1:3 lymphocyte:bead ratio. CD3/CD28 beads

433 were magnetically removed from the culture on day 5 and CAR T-cells rested for 48 h before
434 proceeding to antigen stimulation.
435
436 **CAR construct generation**
437
438 CD19 FMC63 and CAT CAR transfer vectors were generated as previously described[11] and were
439 provided by P.J.A.. The vector structure is schematised in Supplementary Fig. 1a.
440
441 **Lentiviral production by transient transfection**
442
443 Lentiviral production was performed by transient transfection according to the following procedure.
444 The day before transfection, 5.5 x 10^6 293T cells were seeded per 175 cm^2 flasks in complete DMEM,
445 high glucose, GlutaMAX™ Supplement (Gibco™, Thermo Fisher Scientific) supplemented with 10%
446 FBS.
447 To generate viral particles, 293T cells were co-transfected with second generation LV packaging
448 plasmids pMD2.G and pCMV-dR8.74 (plasmidFactory, Bielefeld, Germany) and CAR transfer vectors
449 using GeneJuice® Transfection Reagent (Merck-KGaA, Darmstadt, Germany) according to
450 manufacturer's recommendations. LV supernatants were collected at 48 and 72 h post-transfection,
451 pooled, filtered and stored at -80°C before use.
452
453 **Lentiviral transduction of T-cells**
454
455 Following overnight activation with CD3/CD28 beads, 0.5 x 10^6 beads-activated T-cells were
456 suspended in 0.5 ml of TexMACS, transduced to express CD19 CAR construct (FMC63 or CAT) with 1
457 ml of LV supernatant in RetroNectin® (Takara Bio, Kusatsu, Shiga, Japan)-coated 24-well plates and
458 spinoculated at 1,000 g for 40 min at room temperature. Generally, 2-10 x 10^6 beads-activated T-cells
459 per donor per construct were seeded for transduction. Transduction efficiency was assessed by FACS
460 evaluating mCherry (LV fluorescent marker) expression, at day 8 (7 days after transduction). The
461 copies of lentiviral vectors integrated in the human genome (vector copy number, VCN) were
462 quantified at day 11 (10 days after transduction) using a TaqMan real-time PCR assay targeting the
463 woodchuck hepatitis virus post-transcriptional regulatory element (WPRE) in the LV construct and the
464 human beta-actin gene (Integrated DNA Technologies, Coralville, Iova, USA).
465 UNTR beads-activated T-cells per each donor were used as a control throughout the experiment and
466 were subjected to the same experimental conditions as LV-transduced ones.

467

468 **NALM6 and CAR T-cells co-cultures**

469

470 To assess the anti-tumour activity of CD19 CAR T-cells, we set-up co-cultures with CD19-expressing
471 NALM6 for 24 or 96 h (stimulated conditions) on day 7 (6 days after transduction and 2 days post-
472 CD3/CD28 beads removal). Briefly, beads-activated T-cells were incubated for 48 h in optimised T-cell
473 medium before stimulation. 0.1 x 10^6 UNTR or FMC63 or CAT beads-activated T-cells were seeded in
474 96-well plates in complete TexMACS medium in a 1:1 ratio with irradiated (40 Gy) NALM6. Generally,
475 0.1-6 x 10^6 beads-activated T-cells per donor per condition (UNTR, FMC63 and CAT) were stimulated.
476 Unstimulated, beads-activated T-cells per each donor, condition and time point were kept in culture
477 under the same experimental conditions as antigen-stimulated T-cells.

478

479 **Flow cytometry activated cell sorting and antibody staining**

480

481 All FACS experiments included Fluorescence minus one (FMO) and single-antibody stained BD™
482 CompBeads (BD Biosciences) controls to set expression threshold and to calculate compensation,
483 respectively. Live cells were selected based on their non-permeability and lack of fluorescence
484 associated with DAPI Solution (BD Biosciences, Franklin Lakes, NJ, USA) or 7-AAD Viability Staining
485 Solution (BioLegend, San Diego, CA, USA). The combination of monoclonal antibodies used to identify
486 T-cell subsets is described in the main text. Following 24 or 96 h of stimulation, the phenotype of live
487 T-/CAR T-lymphocytes in all the experimental conditions was assessed using the following antibodies:
488 BV510-anti CD3 (clone OKT3, BioLegend), APC-CY7-anti CD3 (clone UCHT1, BioLegend), APC-CY7-anti
489 CD4, FITC-anti CD4 (clone SK3, BioLegend), PerCP/CY5.5-anti CD8, BV510-anti CD8 (clone RPA-T8,
490 BioLegend), AF647-anti CD62L, APC-anti CD62L (clone DREG-56, BioLegend), BV785-anti CD45RA
491 (clone HI100, BioLegend), V450-anti CD45RA (clone HI100, BD Biosciences), AF647-anti TIM3 (clone
492 7D3, BD Biosciences), BB515-anti PD1 (clone EH12.1, BD Biosciences), BV605-anti LAG3 (clone
493 11C3C65, BioLegend).
494 PBMCs were labelled with PE-anti CD19 (clone HIB19; BioLegend) to detect B-cells in the samples soon
495 after isolation and to check purity after CD19-depletion.
496 For CAR staining, CAR T-cells were incubated with CD19 CAR Detection Reagent human, Biotin
497 (Miltenyi Biotec) followed by incubation with APC-anti biotin Antibody, REAfinity™ (Miltenyi Biotec)
498 and BV510-anti CD3 (clone OKT3; BioLegend) according to manufacturer's recommendations.

499 Experiments were performed on a cell sorter FACSAria™ III (BD Biosciences) and on a CytoFLEX
500 analyzer (Beckman Coulter Inc., Brea, CA, USA) and analysed with FlowJo™ software v10.6.1 (BD
501 Biosciences) and Cytobank platform (www.cytobank.org).
502
503 **RNA sequencing libraries preparation and sequencing**
504
505 RNA sequencing libraries were generated from 8 donors (HD1-HD8), across six experimental
506 conditions, UNTR T-cells or FMC63 or CAT CAR T-cells in either absence or presence of NALM6
507 (unstimulated or stimulated). 1,000 T-cells/CAR T-cells were FACS-sorted in single PCR tubes
508 containing 4 ul of QIAGEN lysis buffer from QIAseq FX Single Cell RNA Library Kit (QIAGEN, Hilden,
509 Germany) and stored at -80°C. The kit steps include reverse transcription, cDNA amplification and
510 PCR-free NGS library preparation. Libraries were purified using AMPure XP magnetic beads (Beckman
511 Coulter Inc.,) according to the manufacturer instructions. After beads purification the libraries were
512 resuspended in 50 µL of buffer EB (Qiagen) and stored at -20 °C. Size and concentration of the libraries
513 generated was assessed using High Sensitivity Bioanalyzer (Agilent, Santa Clara, CA, USA) and Qubit
514 High-Sensitivity DNA kit (Invitrogen™, Thermo Fisher Scientific), respectively. Libraries were
515 equimolarly pooled to a final concentration of 10 nM and were sequenced with Illumina HiSeq 3000
516 (150 bp pair-end reads) at UCL Genomics.
517
518 **RNA sequencing analysis**
519
520 Sequencing quality control and mapping was performed on Fedora 32. DGE analysis and downstream
521 analyses were performed in *R 4.0.2* on Windows 10 (build 18362). Additional details can be found in
522 the transcriptomic Supplementary Bioinformatics Material (SBM). An FDR smaller than 0.1 (when
523 multiple tests were performed) or a *P* value smaller than 0.05 (when only one test was performed)
524 was considered statistically significant. Quality control and adapters trimming was performed with
525 *FastQC 0.11.9*[47] and *cutadapt 2.10*[48]. Sequences were mapped with *STAR 2.7.3a*[49] to the release 31 of
526 the Human Genome (GRCh38.p12)[50] and summarised with *featureCounts* from the *subread 2.0.0*
527 software package[51]. Only genes annotated as protein-coding genes were included into the DE and
528 downstream analyses. These were further filtered by the *filterByExpr* function from the *edgeR*
529 package[52] in order to remove lowly expressed genes. DE was assessed with *DESeq2*[53]. FDR were
530 calculated using Benjamini-Hochberg correction[54].
531 Only the genes which passed the *filterByExpr* filtering were used for GSEA pathway analysis. GSEA was
532 performed with *fgsea* package[55] on a subset of pathways from the MSigDB's Hallmarks pathways[56]

533 (see SBM Table III). The log_2Fold Change of the DE conditions compared with their matched UNTR
534 condition was used as an input of the analysis. Relative cell type enrichment was performed with
535 *xCell*[57] on a subset of cell types (SBM Table IV).
536
537 **Mass cytometry analysis**
538
539 Following 24 h of stimulation, samples in all experimental conditions were treated with Brefeldin A
540 (BioLegend) (1:1,000) at 37°C for 4 h to favour intracellular cytokine accumulation and were fixed with
541 1.6% of formaldehyde for 10 min at room temperature. Fixed samples were stained with 0.05 µM Cell-
542 ID™ Cisplatin-194-Pt (Fluidigm, South San Francisco, CA, USA), a live-dead marker, for 1 min on a
543 rocker. Samples for all experimental conditions from a given donor were then barcoded using the Cell-
544 ID™ 20-Plex Pd Barcoding Kit (Fluidigm) according to manufacturer's instructions. 12-16 samples were
545 labelled concurrently in the same tube following a three-step staining protocol. Briefly, 2.6-5 x 10^6
546 cells were firstly stained with antibodies against surface markers (CD3, CD4, CD8a, CD19, CD22, CD25,
547 CD44, CD45RA, CD62L, CD69, CD127, HLA-DR and TIM-3). Following permeabilization with
548 eBioscience™ Foxp3/Transcription Factor Staining Buffer Set (Thermo Fisher Scientific) for 30 min at
549 4°C, cells were subsequently stained for the detection of intracellular cytokines (IL-4, IL-5, IL-6, IL-23,
550 IL-17A, IL-2, TNF-α, IFN-γ, GM-CSF, TGF-β, Granzyme B and Perforin B) and cytoplasmic protein (RFP
551 and mCherry, used to detect mCherry expression). Cells were then fixed in ice-cold 50% Methanol for
552 10 min at 4°C and underwent antibody staining for nuclear targets (cleaved Caspase 3, Cyclin B1,
553 FOXP3 and NFAT1) and phosphoproteins (p4E-BP1, pAMPKa, pBAD, pBTK, pCREB, pERK1/2, pHistone
554 H2A.X, pHistone H3, pMKK3/MKK6, pp38, pPDPK1, pRB, pS6, pSRC, pSTAT4, pSTAT5 and pZAP70). Two
555 independent mass cytometry experiments were performed and the antibodies used are listed in
556 Supplementary Table 3. Stained cells were fixed with 1.6% of formaldehyde for 10 min at room
557 temperature on a rocker and incubated with Cell-ID™ Intercalator-Ir (Fluidigm) overnight at 4°C. The
558 following day, experiments were performed on a Helios mass cytometer (Fluidigm). EQ™ Four
559 Element Calibration Beads (Fluidigm) were added to cell suspensions immediately before acquisition
560 to guarantee inter-sample comparability.
561
562 **Mass cytometry data pre-processing and analysis**
563
564 The resulting FCS files were normalised against EQ™ Four Element Calibration Beads, debarcoded and
565 uploaded on Cytobank platform. Viable single-cells were cleaned based on Gaussian parameters
566 (Event length, Centre, Offset and Residual), DNA content (193-Ir DNA) and Cisplatin (194-Pt) and gated

567 on CD19, CD3 and mCherry markers to detect B-cells and T-/CAR T-lymphocytes. Cell populations were
568 exported from Cytobank and computationally analysed in Python (Python version 3.7.6) or in R (R
569 version 3.6.1) as described below.
570 Specifically, EMD[17] scores used for PCA were computed separately for each stimulation condition
571 between CAR T-lymphocytes and UNTR T-lymphocytes and the entire population as previously
572 described[58] using CyGNAL repository (10.5281/zenodo.4587193).
573 The PCA performed on EMD scores of all 32 markers and the event counts in CD3+ T-cells from HD4-
574 HD8 across all the experimental conditions highlighted the lack of activation of HD6 CAR T-cells upon
575 antigen stimulation (data not shown). For this reason, HD6 was excluded from the analyses. PCA in
576 Fig. 2b was generated on EMD scores of all 32 markers calculated on CD3+ T-cells across all
577 experimental conditions at 24 h post-stimulation.
578 EMD[17] scores in Fig. 2e, 3e, 4a, 5c-d, Supplementary Fig. 3c, 5-10 were computed separately for each
579 given donor, stimulation condition and manufacture condition between CAR T-lymphocytes and the
580 corresponding UNTR T-cell population.
581 For the comparison between CAR T-cell constructs (Fig. 2e, 3e, 4 and Supplementary Fig. 3c) and
582 between stimulation conditions (Supplementary Fig. 5 and 6) in the standard manufacture condition,
583 only the markers targeted with the same mass cytometry antibody between the two experiments
584 were investigated.
585 Additionally, pre-gated FCS files were imported in R, arcsinh transformed (cofactor = 5) and cell
586 clustered using the R packages *FlowSOM*[40] and *ConsensusClusterPlus*[59] as computed in[60]. The code for
587 the dimensional reduction analysis provided[60] was modified using R package *umap* for UMAP analysis.
588 UMAP analyses were performed downsampling at 1,000 cells and using default parameters.
589 Cytokine co-expression analysis was computed in R on CAR T (CD3+mCherry+) and UNTR (CD3+) T pre-
590 gated FCS files concatenated per donor for each given experimental condition. An expression
591 threshold of 1 was set for all the arcsinh transformed cytokine markers except for TGF-ß, for which a
592 threshold of 4 was selected. Chord diagrams of cytokine co-expression were created with the R
593 package *circlize*[61].
594
595 **Statistical analyses**
596
597 Data are shown as mean ± standard error (se) and statistical analyses were performed in R calculating
598 Paired samples t-tests across experimental conditions unless otherwise stated.
599 EMD-related statistical analyses between selected experimental conditions and the results of
600 polyfunctionality analysis are reported in Supplementary Table 5.

601

602 **Data availability**

603

604 The RNA sequencing data and analyses are available at NCBI's Gene Expression Omnibus (GEO) data
605 repository with the accession code GSE157584 and in GitHub
606 (https://github.com/EduardoGCCM/CATvsFMC63_Michelozzi).
607 Mass cytometry raw and processed data will be made publicly available at
608 https://community.cytobank.org/.

609

610 **References**

611

612 1. Miliotou, A.N. & Papadopoulou, L.C. CAR T-cell Therapy: A New Era in Cancer
613 Immunotherapy. *Curr Pharm Biotechnol* **19**, 5-18 (2018).
614 2. Pehlivan, K.C., Duncan, B.B. & Lee, D.W. CAR-T Cell Therapy for Acute
615 Lymphoblastic Leukemia: Transforming the Treatment of Relapsed and Refractory
616 Disease. *Curr Hematol Malig Rep* **13**, 396-406 (2018).
617 3. Lee, D.W., *et al.* Current concepts in the diagnosis and management of cytokine release
618 syndrome. *Blood* **124**, 188-195 (2014).
619 4. Gust, J., *et al.* Endothelial Activation and Blood-Brain Barrier Disruption in
620 Neurotoxicity after Adoptive Immunotherapy with CD19 CAR-T Cells. *Cancer Discov*
621 **7**, 1404-1419 (2017).
622 5. Watanabe, K., Kuramitsu, S., Posey, A.D., Jr. & June, C.H. Expanding the Therapeutic
623 Window for CAR T Cell Therapy in Solid Tumors: The Knowns and Unknowns of
624 CAR T Cell Biology. *Front Immunol* **9**, 2486 (2018).
625 6. Kowolik, C.M., *et al.* CD28 costimulation provided through a CD19-specific chimeric
626 antigen receptor enhances in vivo persistence and antitumor efficacy of adoptively
627 transferred T cells. *Cancer Res* **66**, 10995-11004 (2006).
628 7. Singh, A.P., *et al.* Development of a quantitative relationship between CAR-affinity,
629 antigen abundance, tumor cell depletion and CAR-T cell expansion using a multiscale
630 systems PK-PD model. *MAbs* **12**, 1688616 (2020).
631 8. Chmielewski, M., Hombach, A., Heuser, C., Adams, G.P. & Abken, H. T cell activation
632 by antibody-like immunoreceptors: increase in affinity of the single-chain fragment
633 domain above threshold does not increase T cell activation against antigen-positive
634 target cells but decreases selectivity. *J Immunol* **173**, 7647-7653 (2004).
635 9. Caruso, H.G., *et al.* Tuning Sensitivity of CAR to EGFR Density Limits Recognition
636 of Normal Tissue While Maintaining Potent Antitumor Activity. *Cancer Res* **75**, 3505-
637 3518 (2015).
638 10. Liu, X., *et al.* Affinity-Tuned ErbB2 or EGFR Chimeric Antigen Receptor T Cells
639 Exhibit an Increased Therapeutic Index against Tumors in Mice. *Cancer Res* **75**, 3596-
640 3607 (2015).
641 11. Ghorashian, S., *et al.* Enhanced CAR T cell expansion and prolonged persistence in
642 pediatric patients with ALL treated with a low-affinity CD19 CAR. *Nat Med* **25**, 1408-
643 1414 (2019).

644 12. Roddie, C., *et al.* Durable Responses and Low Toxicity After Fast Off-Rate CD19
645 Chimeric Antigen Receptor-T Therapy in Adults With Relapsed or Refractory B-Cell
646 Acute Lymphoblastic Leukemia. *J Clin Oncol*, JCO2100917 (2021).
647 13. Valitutti, S., Muller, S., Cella, M., Padovan, E. & Lanzavecchia, A. Serial triggering of
648 many T-cell receptors by a few peptide-MHC complexes. *Nature* **375**, 148-151 (1995).
649 14. Michelozzi, I.M., *et al.* High-dimensional functional phenotyping of preclinical human
650 CAR T cells using mass cytometry. *STAR Protoc* **3**, 101174 (2022).
651 15. Wang, X., *et al.* Phase 1 studies of central memory-derived CD19 CAR T-cell therapy
652 following autologous HSCT in patients with B-cell NHL. *Blood* **127**, 2980-2990
653 (2016).
654 16. Wang, X., *et al.* Comparison of naive and central memory derived CD8(+) effector cell
655 engraftment fitness and function following adoptive transfer. *Oncoimmunology* **5**,
656 e1072671 (2016).
657 17. Orlova, D.Y., *et al.* Earth Mover's Distance (EMD): A True Metric for Comparing
658 Biomarker Expression Levels in Cell Populations. *PLoS One* **11**, e0151859 (2016).
659 18. Fuzzy Analysis (Program FANNY). in *Finding Groups in Data* 164-198 (1990).
660 19. Gomes-Silva, D., *et al.* Tonic 4-1BB Costimulation in Chimeric Antigen Receptors
661 Impedes T Cell Survival and Is Vector-Dependent. *Cell Rep* **21**, 17-26 (2017).
662 20. Frigault, M.J., *et al.* Identification of chimeric antigen receptors that mediate
663 constitutive or inducible proliferation of T cells. *Cancer Immunol Res* **3**, 356-367
664 (2015).
665 21. Long, A.H., *et al.* 4-1BB costimulation ameliorates T cell exhaustion induced by tonic
666 signaling of chimeric antigen receptors. *Nat Med* **21**, 581-590 (2015).
667 22. Singh, N., *et al.* Antigen-independent activation enhances the efficacy of 4-1BB-
668 costimulated CD22 CAR T cells. *Nat Med* **27**, 842-850 (2021).
669 23. Wang, Y., *et al.* Low-dose decitabine priming endows CAR T cells with enhanced and
670 persistent antitumour potential via epigenetic reprogramming. *Nat Commun* **12**, 409
671 (2021).
672 24. Allan, S.E., *et al.* Activation-induced FOXP3 in human T effector cells does not
673 suppress proliferation or cytokine production. *Int Immunol* **19**, 345-354 (2007).
674 25. Ran, Q., *et al.* CRIF1 interacting with CDK2 regulates bone marrow
675 microenvironment-induced G0/G1 arrest of leukemia cells. *PLoS One* **9**, e85328
676 (2014).
677 26. Soroosh, P., Ine, S., Sugamura, K. & Ishii, N. OX40-OX40 ligand interaction through
678 T cell-T cell contact contributes to CD4 T cell longevity. *J Immunol* **176**, 5975-5987
679 (2006).
680 27. Sabatos, C.A., *et al.* A synaptic basis for paracrine interleukin-2 signaling during
681 homotypic T cell interaction. *Immunity* **29**, 238-248 (2008).
682 28. Thurley, K., Gerecht, D., Friedmann, E. & Hofer, T. Three-Dimensional Gradients of
683 Cytokine Signaling between T Cells. *PLoS Comput Biol* **11**, e1004206 (2015).
684 29. Castellino, F., *et al.* Chemokines enhance immunity by guiding naive CD8+ T cells to
685 sites of CD4+ T cell-dendritic cell interaction. *Nature* **440**, 890-895 (2006).
686 30. Hugues, S., *et al.* Dynamic imaging of chemokine-dependent CD8+ T cell help for
687 CD8+ T cell responses. *Nat Immunol* **8**, 921-930 (2007).
688 31. Sheih, A., *et al.* Clonal kinetics and single-cell transcriptional profiling of CAR-T cells
689 in patients undergoing CD19 CAR-T immunotherapy. *Nat Commun* **11**, 219 (2020).
690 32. Bai, Z., *et al.* Single-cell multiomics dissection of basal and antigen-specific activation
691 states of CD19-targeted CAR T cells. *J Immunother Cancer* **9**(2021).

692 33. Holling, T.M., van der Stoep, N., Quinten, E. & van den Elsen, P.J. Activated human
693 T cells accomplish MHC class II expression through T cell-specific occupation of class
694 II transactivator promoter III. *J Immunol* **168**, 763-770 (2002).
695 34. Gourley, T.S. & Chang, C.H. Cutting edge: the class II transactivator prevents
696 activation-induced cell death by inhibiting Fas ligand gene expression. *J Immunol* **166**,
697 2917-2921 (2001).
698 35. Betts, M.R.*, et al.* HIV nonprogressors preferentially maintain highly functional HIV-
699 specific CD8+ T cells. *Blood* **107**, 4781-4789 (2006).
700 36. Caccamo, N.*, et al.* Multifunctional CD4(+) T cells correlate with active
701 Mycobacterium tuberculosis infection. *Eur J Immunol* **40**, 2211-2220 (2010).
702 37. Rossi, J.*, et al.* Preinfusion polyfunctional anti-CD19 chimeric antigen receptor T cells
703 are associated with clinical outcomes in NHL. *Blood* **132**, 804-814 (2018).
704 38. Xhangolli, I.*, et al.* Single-cell Analysis of CAR-T Cell Activation Reveals A Mixed
705 TH1/TH2 Response Independent of Differentiation. *Genomics Proteomics*
706 *Bioinformatics* **17**, 129-139 (2019).
707 39. Spiegel, J.Y.*, et al.* CAR T cells with dual targeting of CD19 and CD22 in adult patients
708 with recurrent or refractory B cell malignancies: a phase 1 trial. *Nat Med* **27**, 1419-1431
709 (2021).
710 40. Van Gassen, S.*, et al.* FlowSOM: Using self-organizing maps for visualization and
711 interpretation of cytometry data. *Cytometry A* **87**, 636-645 (2015).
712 41. Rachmilewitz, J. & Lanzavecchia, A. A temporal and spatial summation model for T-
713 cell activation: signal integration and antigen decoding. *Trends Immunol* **23**, 592-595
714 (2002).
715 42. Klesmith, J.R., Wu, L., Lobb, R.R., Rennert, P.D. & Hackel, B.J. Fine Epitope Mapping
716 of the CD19 Extracellular Domain Promotes Design. *Biochemistry* **58**, 4869-4881
717 (2019).
718 43. Weng, N.P., Araki, Y. & Subedi, K. The molecular basis of the memory T cell response:
719 differential gene expression and its epigenetic regulation. *Nat Rev Immunol* **12**, 306-
720 315 (2012).
721 44. Singh, H.*, et al.* Manufacture of clinical-grade CD19-specific T cells stably expressing
722 chimeric antigen receptor using Sleeping Beauty system and artificial antigen
723 presenting cells. *PLoS One* **8**, e64138 (2013).
724 45. Noaks, E., Peticone, C., Kotsopoulou, E. & Bracewell, D.G. Enriching leukapheresis
725 improves T cell activation and transduction efficiency during CAR T processing. *Mol*
726 *Ther Methods Clin Dev* **20**, 675-687 (2021).
727 46. Turtle, C.J.*, et al.* CD19 CAR-T cells of defined CD4+:CD8+ composition in adult B
728 cell ALL patients. *J Clin Invest* **126**, 2123-2138 (2016).
729 47. Andrews, S. FastQC: A quality control tool for high throughput sequence data. (2019).
730 48. Martin, M. Cutadapt removes adapter sequences from high-throughput sequencing
731 reads. *2011* **17**, 3 (2011).
732 49. Dobin, A.*, et al.* STAR: ultrafast universal RNA-seq aligner. *Bioinformatics* **29**, 15-21
733 (2013).
734 50. Frankish, A.*, et al.* GENCODE reference annotation for the human and mouse
735 genomes. *Nucleic Acids Research* **47**, D766-D773 (2018).
736 51. Liao, Y., Smyth, G.K. & Shi, W. featureCounts: an efficient general purpose program
737 for assigning sequence reads to genomic features. *Bioinformatics* **30**, 923-930 (2014).
738 52. Chen, Y., Lun, A. & Smyth, G. From reads to genes to pathways: differential expression
739 analysis of RNA-Seq experiments using Rsubread and the edgeR quasi-likelihood
740 pipeline [version 2; peer review: 5 approved]. *F1000Research* **5**(2016).

741 53. Love, M.I., Huber, W. & Anders, S. Moderated estimation of fold change and
742 dispersion for RNA-seq data with DESeq2. *Genome Biology* **15**, 550 (2014).
743 54. Benjamini, Y. & Hochberg, Y. Controlling the False Discovery Rate: A Practical and
744 Powerful Approach to Multiple Testing. *Journal of the Royal Statistical Society. Series*
745 *B (Methodological)* **57**, 289-300 (1995).
746 55. Korotkevich, G., Sukhov, V. & Sergushichev, A. Fast gene set enrichment analysis.
747 *bioRxiv*, 060012 (2019).
748 56. Liberzon, A.*, et al.* The Molecular Signatures Database (MSigDB) hallmark gene set
749 collection. *Cell Syst* **1**, 417-425 (2015).
750 57. Aran, D., Hu, Z. & Butte, A.J. xCell: digitally portraying the tissue cellular
751 heterogeneity landscape. *Genome Biol* **18**, 220 (2017).
752 58. Qin, X.*, et al.* Cell-type-specific signaling networks in heterocellular organoids. *Nat*
753 *Methods* **17**, 335-342 (2020).
754 59. Wilkerson, M.D. & Hayes, D.N. ConsensusClusterPlus: a class discovery tool with
755 confidence assessments and item tracking. *Bioinformatics* **26**, 1572-1573 (2010).
756 60. Nowicka, M.*, et al.* CyTOF workflow: differential discovery in high-throughput high-
757 dimensional cytometry datasets. *F1000Res* **6**, 748 (2017).
758 61. Gu, Z., Gu, L., Eils, R., Schlesner, M. & Brors, B. circlize Implements and enhances
759 circular visualization in R. *Bioinformatics* **30**, 2811-2812 (2014).
760

761 **Figure legends**

762 **Fig. 1: Generation and phenotypic characterisation of CAR T-cells from HD-PBMCs.**

763 **a** Experimental workflow. Peripheral Blood Mononuclear Cells (PBMCs) were isolated from HDs and
764 LV transduced to express CD19 CAR construct (FMC63 or CAT) following overnight activation with
765 CD3/CD28 beads. Six days after transduction, CAR T-cells were cultured without (unstimulated) or
766 with target cells (NALM6) at 1:1 ratio (stimulated). Unstimulated and stimulated cells were analysed
767 by flow cytometry and sorted for RNA-sequencing 24 hours post-stimulation. Mass cytometry analysis
768 was performed on unstimulated and stimulated cells at 24 h post-stimulation. Activated UNTR T-cells
769 were used as a control throughout the experiment.

770 **b** (left) Spaghetti plots showing transduction levels of CAR T-cells as percentage of mCherry+ (in CD3+)
771 and (right) as MFI of mCherry in unstimulated transduced T-cells measured by FACS 7 days post-
772 transduction. Lines connect results from individual donors (n= 12 HDs, n = 3 independent
773 experiments).

774 **c** Spaghetti plot showing the percentage of surface CAR expression (in CD3+) in unstimulated
775 transduced T-cells measured by FACS 10 days post-transduction. Lines connect results from individual
776 donors (n = 4 HDs, n = 1 independent experiment).

777 **d** Variation (log2 fold change) of CD4 and CD8 proportion in unstimulated UNTR T-cells and FMC63
778 and CAT CAR T-cells measured by FACS 7 days post-transduction. The dotted horizontal line (0)
779 represents the conditions in which CD4=CD8. Data represent mean ± se (n = 12 HDs, n = 3 independent
780 experiments).

781 **e** (left) Barplots showing the percentage of TCM (CD45RA-CD62L+), (middle) TEM (CD45RA-CD62L-)
782 and (right) TEMRA (CD45RA+CD62L-) in unstimulated CD3+ UNTR T-cells and FMC63 and CAT CAR T-
783 cells measured by FACS 10 days post-transduction. Data represent mean ± se (n = 7 HDs, n = 2
784 independent experiments).
785 **b-e** Statistical significance was calculated by Paired t-test. *P < 0.05, **P < 0.01, ****P < 0.0001.
786 Each experimental condition is indicated by a specific colour code (UNTR light grey, FMC63 light blue,
787 CAT orange).
788
789 **Fig. 2: RNA-seq and mass cytometry analyses of unstimulated untransduced and CAR-transduced T-**
790 **cells.**
791 **a** PCA of the top 500 variable genes from RNA-seq analysis across all the experimental conditions (n =
792 6 HDs, n = 2 independent experiments).
793 **b** PCA of mass cytometry EMD scores computed at 24 h post-stimulation in CD3+ cells across all the
794 experimental conditions (n = 4 HDs, n = 1 independent experiment).
795 **c** Fuzzy clustering analysis of RNA-seq data across all experimental conditions (n = 6 HDs, n = 2
796 independent experiments).
797 **d** (top) Volcano plot showing DE genes between unstimulated FMC63 and CAT CAR T-cells. The dashed
798 horizontal line represents the statistical significance threshold (FDR < 0.1). (bottom) The barplots show
799 the expression of selected DE genes (FDR < 0.1) in unstimulated untransduced and transduced T-cells.
800 Data represent mean ± se (n = 6 HDs, n = 2 independent experiments).
801 **e** The barplots show the expression of mass cytometry EMD scores for Granzyme B, Perforin B, HLA-
802 DR, CD25, NFAT1, pZAP70 and pS6 in unstimulated CAR T-cells at 24 h upon stimulation. The data
803 shown are normalized to stimulated CD3+ UNTR T-cells. The dotted horizontal line (0) represents the
804 expression of a specific marker in unstimulated CD3+ UNTR T-cells. Data represent mean ± se (n = 7
805 HDs, n = 2 independent experiments). Statistical significance was calculated by Paired t-test. *P < 0.05,
806 **P < 0.01.
807 **a-e** Each experimental condition is indicated by a specific colour code (Unstimulated conditions =
808 UNTR light grey, FMC63 light blue, CAT orange; stimulated conditions = UNTR grey, FMC63 blue, CAT
809 red).
810
811 **Fig. 3: Phenotypic and molecular characterisation of stimulated CAR-transduced T-cells.**
812 **a** Variation (log2 fold change) of CD4 and CD8 proportion in stimulated UNTR T-cells and FMC63 and
813 CAT CAR T-cells measured by FACS (n = 12 HDs, n = 3 independent experiments). The dotted horizontal
814 line (0) represents the conditions in which CD4=CD8.

815 **b** Barplot showing the percentage of TCM (CD45RA-CD62L+) in stimulated CD3+ UNTR T-cells and
816 FMC63 and CAT CAR T-cells measured by FACS 96h post-antigen stimulation (n = 7 HDs, n = 2
817 independent experiments).
818 **c** Barplots showing the expression of T-cell exhaustion markers (PD1, TIM3 and LAG3) as MFI in
819 stimulated CD3+ UNTR T-cells and FMC63 and CAT CAR T-cells measured by FACS 96h post-antigen
820 stimulation (n = 4 HDs, n = 1 independent experiment).
821 **d** (left) Volcano plot showing DE genes between FMC63 and CAT CAR T-cells upon NALM6 co-culture.
822 The dashed horizontal line represents the statistical significance threshold (FDR < 0.1). (right) The
823 barplots show the expression of selected DE genes (FDR < 0.1) in stimulated UNTR T-cells and in CAR
824 T-cells (n = 6 HDs, n = 2 independent experiments).
825 **e** The barplots show the expression of mass cytometry EMD scores for CD25, HLA-DR, NFAT1, FOXP3,
826 pZAP70, pS6, pp38, pCREB, pRB and CD4 in stimulated CAR T-cells at 24 h upon stimulation. The data
827 shown are normalized to stimulated CD3+ UNTR T-cells. The dotted horizontal line (0) represents the
828 expression of a specific marker in stimulated CD3+ UNTR T-cells. (n = 7 HDs, n = 2 independent
829 experiments).
830 **a-e** Barplots show mean ± se. Each experimental condition is indicated by a specific colour code (UNTR
831 grey, FMC63 blue, CAT red).
832 **a, b, c, e** Statistical significance was calculated by Paired t-test. *P < 0.05, **P < 0.01, ***P < 0.001,
833 ****P < 0.0001.
834
835 **Fig. 4: Cytokine polyfunctionality in stimulated CAR-transduced T-cells.**
836 **a** The barplots show the expression of mass cytometry EMD scores for effector (Granzyme B, IFN-γ,
837 TNF-α) and stimulatory (GM-CSF, IL-2) cytokines in stimulated CAR T-cells. The data shown are
838 normalized to stimulated CD3+ UNTR T-cells. The dotted horizontal line (0) represents the expression
839 of a specific marker in stimulated CD3+ UNTR T-cells. (n = 7 HDs, n = 2 independent experiments).
840 **b** Barplots showing the mean cytokine polyfunctionality in stimulated CAR T-cells, normalized to
841 stimulated CD3+ UNTR T -cells. The dotted horizontal line (1) represents the mean polyfunctionality
842 in stimulated CD3+ UNTR T-cells. (n = 7 HDs, n = 2 independent experiments).
843 **c** The stacked barplots show the percentage of stimulated CAR T cells (CD3+mCherry+) expressing 1
844 to 4 or >=5 cytokines/cell as measured by mass cytometry.
845 **d** The circos plots show all the combinations of the 8 cytokines analysed in stimulated FMC63 (left)
846 and CAT (right) CAR T-cells by mass cytometry. The numbers indicate patterns of cytokine co-
847 expression (from 1 to 4 or >=5 cytokines/cell). A specific colour code has been assigned to each
848 cytokine.

849 **a-b** Data represent mean ± se. Statistical significance was calculated by Paired t-test. *P < 0.05, ***P
850 < 0.001.
851 Each experimental condition is indicated by a specific colour code (FMC63 blue, CAT red).
852
853 **Fig. 5: Molecular characterisation of CAR T-cells generated from CD19-depleted PBMCs.**
854 **a** (left) UMAP representation of the 4 cell populations (CD8, CD4, CD3 low/neg, CD19) identified by
855 FlowSOM analysis in 4 representative unstimulated samples analysed by mass cytometry at 24 h post-
856 stimulation (n = 4 HDs, n = 1 independent experiment). The cell types are indicated by different
857 colours. (right) Percentage of residual B-cells detected by mass cytometry in unstimulated samples at
858 24 h post-stimulation. (n = 7 HDs, n = 2 independent experiments).
859 **b** (left) Barplots showing the percentage of TCM (CD45RA-CD62L+) and (right) TEM (CD45RA-CD62L-)
860 in unstimulated CD19-depleted CD3+ UNTR T-cells and FMC63 and CAT CAR T-cells measured by FACS
861 (n = 4 HDs, n = 1 independent experiment).
862 **c** The barplots show the expression of mass cytometry EMD scores for Granzyme B, Perforin B, HLA-
863 DR, CD25, NFAT1, pZAP70 and pS6 in unstimulated CD19-depleted CAR T-cells at 24 h upon
864 stimulation. The data shown are normalized to stimulated CD3+ UNTR T-cells. The dotted horizontal
865 line (0) represents the expression of a specific marker in unstimulated CD3+ CD19-depleted UNTR T-
866 cells. (n = 3 HDs, n = 1 independent experiment).
867 **d** The barplots show the expression of mass cytometry EMD scores for CD25, HLA-DR, NFAT1, pZAP70,
868 pS6, pp38, pRB and CD4 in stimulated CD19-depleted CAR T-cells at 24 h upon stimulation. The data
869 shown are normalized to stimulated CD3+ UNTR T-cells. The dotted horizontal line (0) represents the
870 expression of a specific marker in stimulated CD19-depleted CD3+ UNTR T-cells. (n = 3 HDs, n = 1
871 independent experiment).
872 **e** Barplots showing the mean polyfunctionality in CD19-depleted CAR T-cells at 24 h upon stimulation.
873 The data shown are normalized to stimulated CD3+ UNTR T-cells. The dotted horizontal line (1)
874 represents the mean polyfunctionality in stimulated CD3+ CD19-depleted UNTR T-cells. (n = 3 HDs, n
875 = 1 independent experiment).
876 **a-e** Each experimental condition is indicated by a specific colour code (Unstimulated conditions =
877 UNTR light grey, FMC63 light blue, CAT orange; stimulated conditions = FMC63 blue, CAT red). Barplots
878 show mean ± se. Statistical significance was calculated by Paired t-test. *P < 0.05, **P < 0.01.
879
880 **Supplementary Fig. 1: Generation and phenotypic characterisation of CAR T-cells from HD-PBMCs.**
881 **a** (left) Schematic representation of the FMC63 and CAT bicistronic lentiviral vector constructs and
882 (right) of FMC63 and CAT CAR structure. Both constructs are second generation CARs composed by an

883 anti-CD19 scFv, derived from FMC63 or CAT13.1E10 hybridoma, a CD8a hinge, a CD8a transmembrane
884 domain (TM), a 4-1BB costimulatory domain and a CD3z signalling domain linked to a reporter gene
885 (mCherry), marker of transduction.
886 **b** The barplots show the vector copy number (VCN) quantification in unstimulated FMC63 and CAT
887 CAR T-cells. Each dot represents an individual donor (mean of technical triplicates). Each experimental
888 condition is indicated by a specific colour code (FMC63 light blue, CAT orange). Data represent mean
889 ± se (n = 4 HDs, n = 1 independent experiment). Statistical significance was calculated by Paired t-test.
890
891 **Supplementary Fig. 2: RNA-seq analyses of unstimulated and stimulated untransduced and CAR**
892 **transduced T-cells.**
893 **a** Correlation of mCherry MFI measured by FACS with normalised RNA-seq counts (CPM) aligning to
894 the scFv region of each of the two CARs (n = 6 HDs, n = 2 independent experiments). Pearson
895 correlation and P values are displayed.
896 **b** Correlation of the percentage of CD4+ T-cells detected by FACS with CD4 mRNA levels (n = 6 HDs,
897 n= 2 independent experiments). Pearson correlation and P values are displayed.
898 **c** Correlation of the percentage of CD8+ T-cells detected by FACS with CD8 mRNA levels (n=6 HDs, n =
899 1 independent experiment). Pearson correlation and P values are displayed.
900 **d** Heatmap showing the hierarchical clustering of all the experimental conditions analysed displaying
901 the top 100 variable genes from RNA-seq PC1 (n = 6 HDs, n = 2 independent experiments).
902 **a-d** Each experimental condition is indicated by a specific colour code (Unstimulated conditions =
903 UNTR light grey, FMC63 light blue, CAT orange; stimulated conditions = UNTR grey, FMC63 blue, CAT
904 red).
905
906 **Supplementary Fig. 3: RNA-seq and mass cytometry analyses of unstimulated and stimulated**
907 **untransduced and CAR-transduced T-cells.**
908 **a** Bar plots of the top contributing variables to PC1 and PC2 in Fig. 2b. The dashed horizontal red line
909 represents the expected average contribution of the variables.
910 **b** GSEA of HALLMARK gene sets for (1) FMC63 or (2) CAT CAR T unstimulated condition vs UNTR
911 unstimulated cells, (3) FMC63 or (4) CAT CAR T stimulated condition vs UNTR stimulated cells (n = 6
912 HDs, n = 2 independent experiments). Non-significant enrichment scores were set to zero. Gene sets
913 with no significant enrichment scores are not shown.
914 **c** The barplots show the expression of mass cytometry EMD scores for GM-CSF and IL-17A in
915 unstimulated CAR T-cells at 24 h upon stimulation. The dotted horizontal line (0) represents the

916 expression of a specific marker in unstimulated CD3+ UNTR T-cells. Data represent mean ± se (n = 7
917 HDs, n = 2 independent experiments). Statistical significance was calculated by Paired t-test. *P < 0.05.
918 **b-c** Each experimental condition is indicated by a specific colour code (Unstimulated conditions =
919 FMC63 light blue, CAT orange; stimulated conditions = FMC63 blue, CAT red).
920
921 **Supplementary Fig. 4: Phenotypic and molecular characterisation of stimulated CAR T-cells.**
922 **a** (left) Percentage of CD8+ cells in unstimulated and stimulated UNTR T-cells and FMC63 and CAT CAR
923 T-cells. (right) Percentage of CD4+ cells in unstimulated and stimulated UNTR T-cells and FMC63 and
924 CAT CAR T-cells (n = 12 HDs, n = 3 independent experiments). Statistical significance was calculated by
925 Paired t-test. ***P < 0.001, ****P < 0.0001.
926 **b** The barplots show the expression of selected DE genes (FDR < 0.1) in stimulated untransduced and
927 transduced T-cells (n = 6 HDs, n = 2 independent experiments).
928 **a-b** Barplots show mean ± se. Each experimental condition is indicated by a specific colour code
929 (Unstimulated conditions = UNTR light grey, FMC63 light blue, CAT orange; stimulated conditions =
930 UNTR grey, FMC63 blue, CAT red).
931
932 **Supplementary Fig. 5: Mass cytometry EMD scores in unstimulated and stimulated CAT CAR**
933 **transduced T-cells.**
934 The barplots show mass cytometry EMD scores for activation/proliferation markers and
935 cytokines differentially expressed between unstimulated and stimulated CAT CAR T-cells. The dotted
936 horizontal line (0) represents the expression of a specific marker in the UNTR condition, used as a
937 reference. (n = 7 HDs, n = 2 independent experiments).
938 Data represent mean ± se. Statistical significance was calculated by Paired t-test. *P < 0.05, **P < 0.01,
939 ***P < 0.001.
940 Each experimental condition is indicated by a specific colour code (Unstimulated condition orange;
941 stimulated condition red).
942
943 **Supplementary Fig. 6: Mass cytometry EMD scores in unstimulated and stimulated FMC63 CAR**
944 **transduced T-cells.**
945 The barplots show mass cytometry EMD scores for activation and proliferation markers
946 differentially expressed between unstimulated and stimulated FMC63 CAR T-cells. The dotted
947 horizontal line (0) represents the expression of a specific marker in the UNTR condition, used as a
948 reference. (n = 7 HDs, n = 2 independent experiments).
949 Data represent mean ± se. Statistical significance was calculated by Paired t-test. *P < 0.05, **P < 0.01.

950 Each experimental condition is indicated by a specific colour code (Unstimulated condition light blue;
951 stimulated condition blue).
952
953 **Supplementary Fig. 7: Phenotypic and molecular characterisation of untransduced and transduced**
954 **T-cells derived from CD19-depleted PBMCs.**
955 **a** UMAP showing the expression of selected markers (CD3, CD19) detected by mass cytometry at 24 h
956 post-stimulation in unstimulated CD3+ cells across all the experimental conditions (n=4 HDs, n=1
957 independent experiment). The colour scale reflects the protein expression levels.
958 **b** The barplots show the percentage of B-cells detected at FACS at day 0 in freshly isolated PBMCs or
959 in CD19-depleted PBMCs (n = 12 HDs, n = 3 independent experiments).
960 **c** (left) Spaghetti plots showing transduction levels of CAR T-cells as percentage of mCherry+ (in CD3+)
961 and (right) as MFI of mCherry in unstimulated transduced CD19-depleted T-cells measured by FACS at
962 7 days post-transduction. Lines connect results from individual donors (n= 4 HDs, n = 1 independent
963 experiment).
964 **d** The barplots show the integrated vector copy number (VCN) in unstimulated CD19-depleted FMC63
965 and CAT CAR T-cells. Each dot represents an individual donor (mean of technical duplicates) (n= 4 HDs,
966 n = 1 independent experiment).
967 **e** Variation (log2 fold change) of CD4 and CD8 proportion in unstimulated CD19-depleted UNTR T-cells
968 and FMC63 and CAT CAR T-cells measured by FACS. The dotted horizontal line (0) represents the
969 conditions in which CD4=CD8. (n=4 HDs, n=1 independent experiment).
970 **f** The barplots show the expression of mass cytometry EMD scores for CD69 and pRB in unstimulated
971 CD19-depleted CAR T-cells at 24 h upon stimulation. The dotted horizontal line (0) represents the
972 expression of a specific marker in unstimulated CD3+ CD19-depleted UNTR T-cells. (n = 3 HDs, n = 1
973 independent experiment).
974 **g** (left) Variation (log2 fold change) of CD4 and CD8 proportion in stimulated CD19-depleted UNTR T-
975 cells and FMC63 and CAT CAR T-cells measured by FACS. The dotted horizontal line (0) represents the
976 conditions in which CD4=CD8. (middle) Percentage of CD8+ cells in unstimulated and stimulated CD19-
977 depleted UNTR T-cells and FMC63 and CAT CAR T-cells. (right) Percentage of CD4+ cells in
978 unstimulated and stimulated CD19-depleted UNTR T-cells and FMC63 and CAT CAR T-cells (n = 4 HDs,
979 n = 1 independent experiment).
980 **h** Barplots showing the expression of T-cell exhaustion markers (PD1, TIM3 and LAG3) as MFI in
981 stimulated CD19-depleted CD3+ UNTR T-cells and FMC63 and CAT CAR T-cells measured by FACS (n =
982 4 HDs, n = 1 independent experiment).

983 **i** The barplots show the expression of mass cytometry EMD scores for FOXP3, pCREB and IL-2 in
984 stimulated CD19-depleted CAR T-cells at 24 h upon stimulation. The dotted horizontal line (0)
985 represents the expression of a specific marker in stimulated CD3+ CD19-depleted UNTR T-cells. (n = 3
986 HDs, n = 1 independent experiment).
987 **b-i** Each experimental condition is indicated by a specific colour code (Unstimulated conditions = UNTR
988 light grey, FMC63 light blue, CAT orange; stimulated conditions = UNTR grey, FMC63 blue, CAT red).
989 Data represent mean ± se. Statistical significance was calculated by Paired t-test. *P < 0.05, **P < 0.01,
990 ****P < 0.0001.
991
992 **Supplementary Fig. 8: Mass cytometry EMD scores in standard or CD19-depleted unstimulated CAT**
993 **CAR transduced T-cells.**
994 The barplots show mass cytometry EMD scores for activation/proliferation markers and
995 cytokines differentially expressed between CAT CAR T-cells manufactured in standard or CD19-
996 depleted conditions. The data shown are normalized to unstimulated CD3 UNTR T cell control. The
997 dotted horizontal line (0) represents the expression of a specific marker in the unstimulated UNTR
998 condition (n = 3 HDs, n = 1 independent experiment).
999 Data represent mean ± se. Statistical significance was calculated by Paired t-test. *P < 0.05, **P < 0.01.
1000 Each experimental condition is indicated by a specific colour code (Standard condition orange; CD19-
1001 depleted condition salmon).
1002
1003 **Supplementary Fig. 9: Mass cytometry EMD scores in standard or CD19-depleted unstimulated**
1004 **FMC63 CAR transduced T-cells.**
1005 The barplots show mass cytometry EMD scores for activation/proliferation markers and
1006 cytokines differentially expressed between FMC63 CAR T-cells manufactured in standard or CD19-
1007 depleted conditions. The data shown are normalized to unstimulated CD3 UNTR T-cell control. The
1008 dotted horizontal line (0) represents the expression of a specific marker in the unstimulated UNTR
1009 condition. (n = 3 HDs, n = 1 independent experiment).
1010 Data represent mean ± se. Statistical significance was calculated by Paired t-test. *P < 0.05, **P < 0.01.
1011 Each experimental condition is indicated by a specific colour code (Standard condition light blue;
1012 CD19-depleted condition cornflower blue).
1013
1014 **Supplementary Fig. 10: Mass cytometry EMD scores in unstimulated and stimulated CD19-depleted**
1015 **CAT CAR transduced T-cells.**
1016 The barplots show mass cytometry EMD scores for activation/proliferation markers and

1017 cytokines differentially expressed between unstimulated and stimulated CAT CAR T-cells
1018 manufactured in CD19-depleted conditions. The data shown are normalized to unstimulated CD3
1019 UNTR T-cell control. The dotted horizontal line (0) represents the expression of a specific marker in
1020 the CD19-depleted UNTR condition. (n = 3 HDs, n = 1 independent experiment).
1021 Data represent mean ± se. Statistical significance was calculated by Paired t-test. *P < 0.05, **P < 0.01,
1022 ***P < 0.001.
1023 Each experimental condition is indicated by a specific colour code (Unstimulated condition orange;
1024 stimulated condition red).
1025
1026 **Supplementary Fig. 11: Mass cytometry EMD scores in unstimulated and stimulated CD19-depleted**
1027 **FMC63 CAR transduced T-cells.**
1028 The barplots show mass cytometry EMD scores for activation and proliferation markers
1029 differentially expressed between unstimulated and stimulated FMC63 CAR T-cells manufactured in
1030 CD19-depleted conditions. The data shown are normalized to unstimulated CD3 UNTR T-cell control.
1031 The dotted horizontal line (0) represents the expression of a specific marker in the UNTR CD19-
1032 depleted condition (n = 3 HDs, n = 1 independent experiment).
1033 Data represent mean ± se. Statistical significance was calculated by Paired t-test. *P < 0.05, ***P <
1034 0.001.
1035 Each experimental condition is indicated by a specific colour code (Unstimulated condition light blue;
1036 stimulated condition blue).
1037
1038
1039 **Acknowledgements**
1040
1041 We are grateful to the UCL ICH Flow Cytometry facility for support in cell-sorting. We are grateful to
1042 Dr Thomas Adejumo (Fluidigm) for mass cytometry valuable suggestions and assistance with protocols
1043 design. We thank Dr Anne Marijn Kramer (Amsterdam UMC) for generating CD19 FMC63 and CAT CAR
1044 transfer vector plasmids with S.G. and M.P. and P.J.A. The authors acknowledge the contribution of
1045 UCL Genomics Facility. This work was supported by the NIHR GOSH BRC (NIHR GOSH BRC 17PA01),
1046 the views expressed are those of the author(s) and not necessarily those of the NHS, the NIHR, or the
1047 Department of Health. Part of this work was supported by the Leukaemia UK John Goldman Fellowship

1048 to A.G. (2018/JGF/003), the Rosetrees Trust fund to A.G. (M700) and the Academy of Medical Sciences
1049 Springboard Award to A.G. (SBF004\1025).
1050
1051 **Author contributions**
1052
1053 I.M.M. designed, performed and analyzed experiments, performed bioinformatic analyses of mass
1054 cytometry experiments and contributed to writing the manuscript. E.G-C performed bioinformatic
1055 analyses of transcriptomic data and wrote the relative bioinformatic supplementary information.
1056 R.V.C.P. performed experiments and bioinformatic analyses of mass cytometry and transcriptomic
1057 data. F.C-R provided data analysis tools and contributed to bioinformatic analyses of mass cytometry
1058 experiments. P.P-C. performed transcriptomic bioinformatic analyses data checks and contributed to
1059 writing the bioinformatic supplementary information. J. S., M.S., S.W.W, A.Gu. and E.K. performed
1060 experiments. A.E. provided support to cell sorting. J.F. provided analytical pipelines and useful
1061 discussion for the analysis and normalization of mass cytometry data. S.G. and M.P. provided CAR
1062 constructs. C.J.T provided expertise in mass cytometry and reagents. P.J.A. provided reagents and
1063 expertise and contributed to writing the manuscript. S.C. supervised the bioinformatic analyses and
1064 contributed to writing the manuscript. A.G. designed and supervised the project, performed and
1065 analyzed experiments and wrote the manuscript. All authors provided critical feedback and helped
1066 shape the research, analysis and manuscript.
1067
1068 **Competing interests**
1069
1070 The authors declare no competing interests.

1071 **Correspondence**
1072
1073 Corrispondence to Dr Alice Giustacchini.

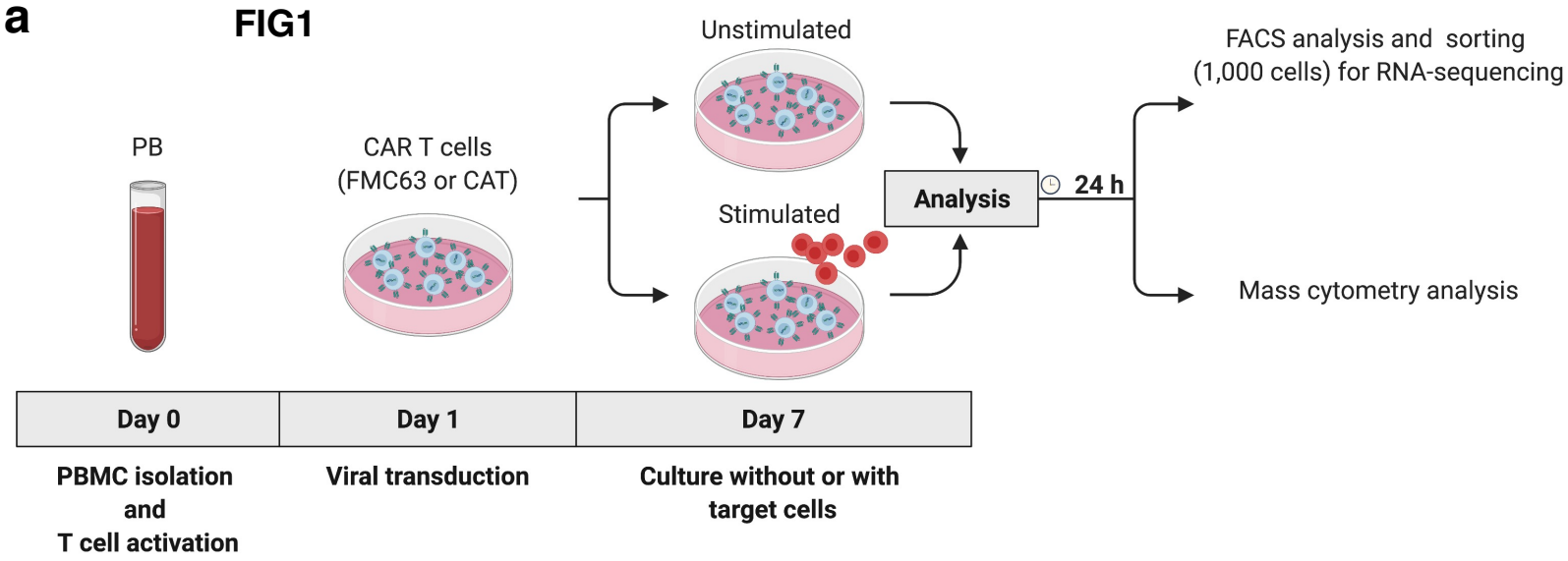
a
FIG1
PB
CAR T cells
(FMC63 or CAT)
Unstimulated
Stimulated
Analysis
24 h
FACS analysis and sorting
(1,000 cells) for RNA-sequencing
Mass cytometry analysis
Day 0
Day 1
Day 7
PBMC isolation
and
T cell activation
Viral transduction
Culture without or with
target cells

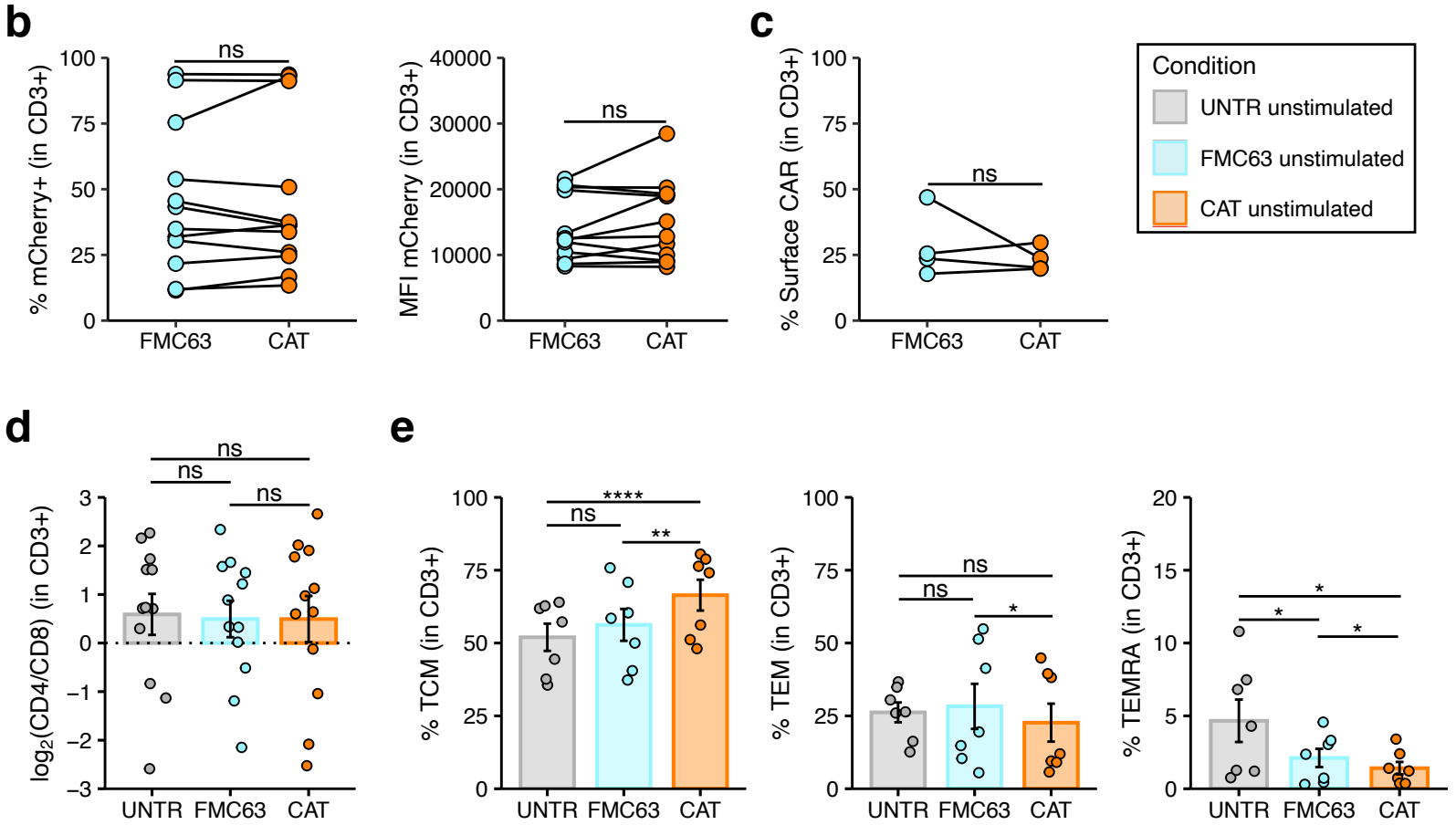
b
% mCherry+ (in CD3+)
MFI mCherry (in CD3+)
ns
FMC63
CAT
c
% Surface CAR (in CD3+)
Condition
UNTR unstimulated
FMC63 unstimulated
CAT unstimulated
d
log2(CD4/CD8) (in CD3+)
UNTR
e
% TCM (in CD3+)
% TEM (in CD3+)
% TEMRA (in CD3+)
****
**
*

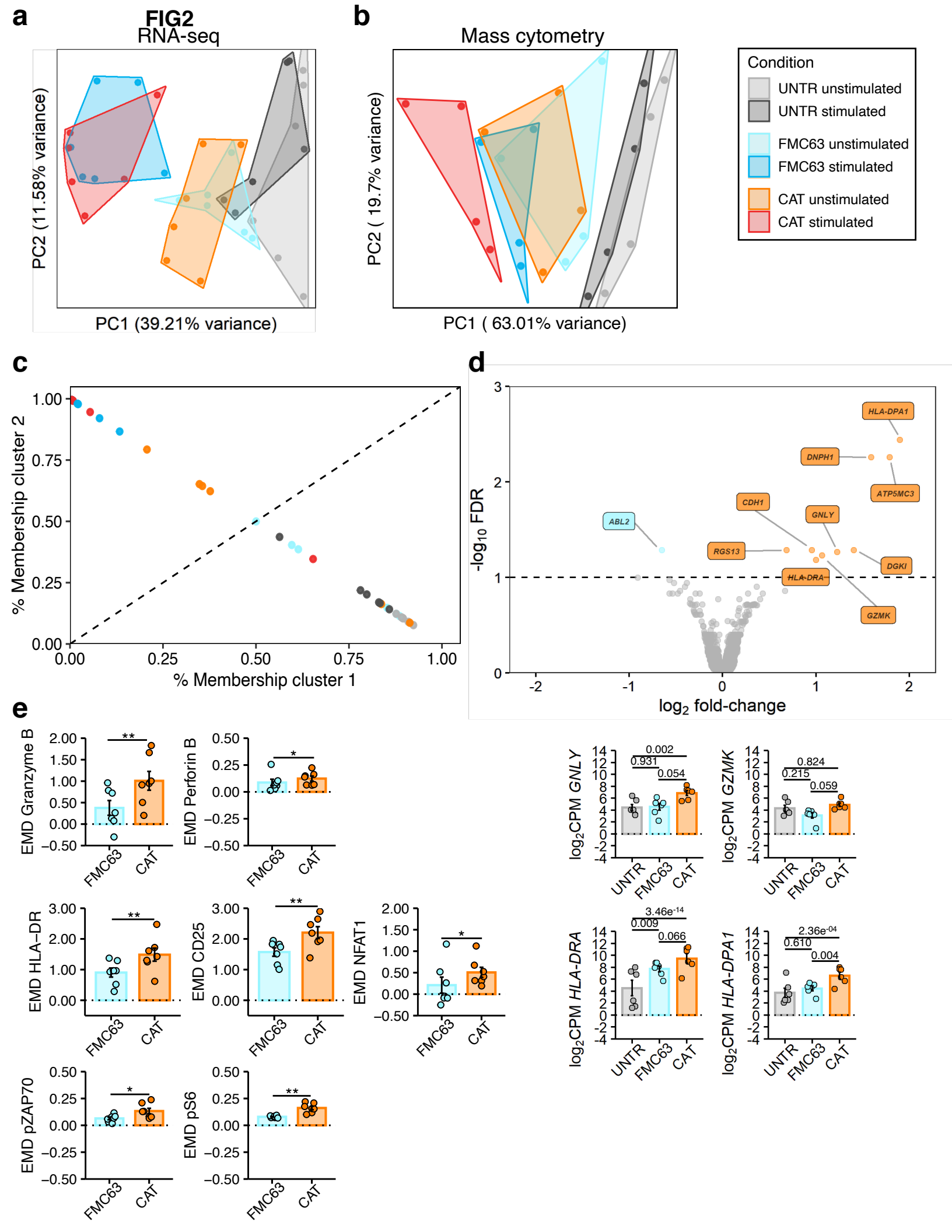
FIG2
a
RNA-seq
PC2 (11.58% variance)
PC1 (39.21% variance)
b
Mass cytometry
PC2 (19.7% variance)
PC1 (63.01% variance)
Condition
UNTR unstimulated
UNTR stimulated
FMC63 unstimulated
FMC63 stimulated
CAT unstimulated
CAT stimulated
c
% Membership cluster 2
% Membership cluster 1
d
-log10 FDR
log2 fold-change
HLA-DPA1
DNPH1
ATP5MC3
CDH1
GNLY
ABL2
RGS13
DGKI
HLA-DRA
GZMK
e
EMD Granzyme B
EMD Perforin B
EMD HLA-DR
EMD CD25
EMD NFAT1
EMD pZAP70
EMD pS6
FMC63
CAT
log2CPM GNLY
log2CPM GZMK
log2CPM HLA-DRA
log2CPM HLA-DPA1
UNTR
0.002
0.931
0.054
0.824
0.215
0.059
3.46e-14
0.009
0.066
2.36e-04
0.610
0.004

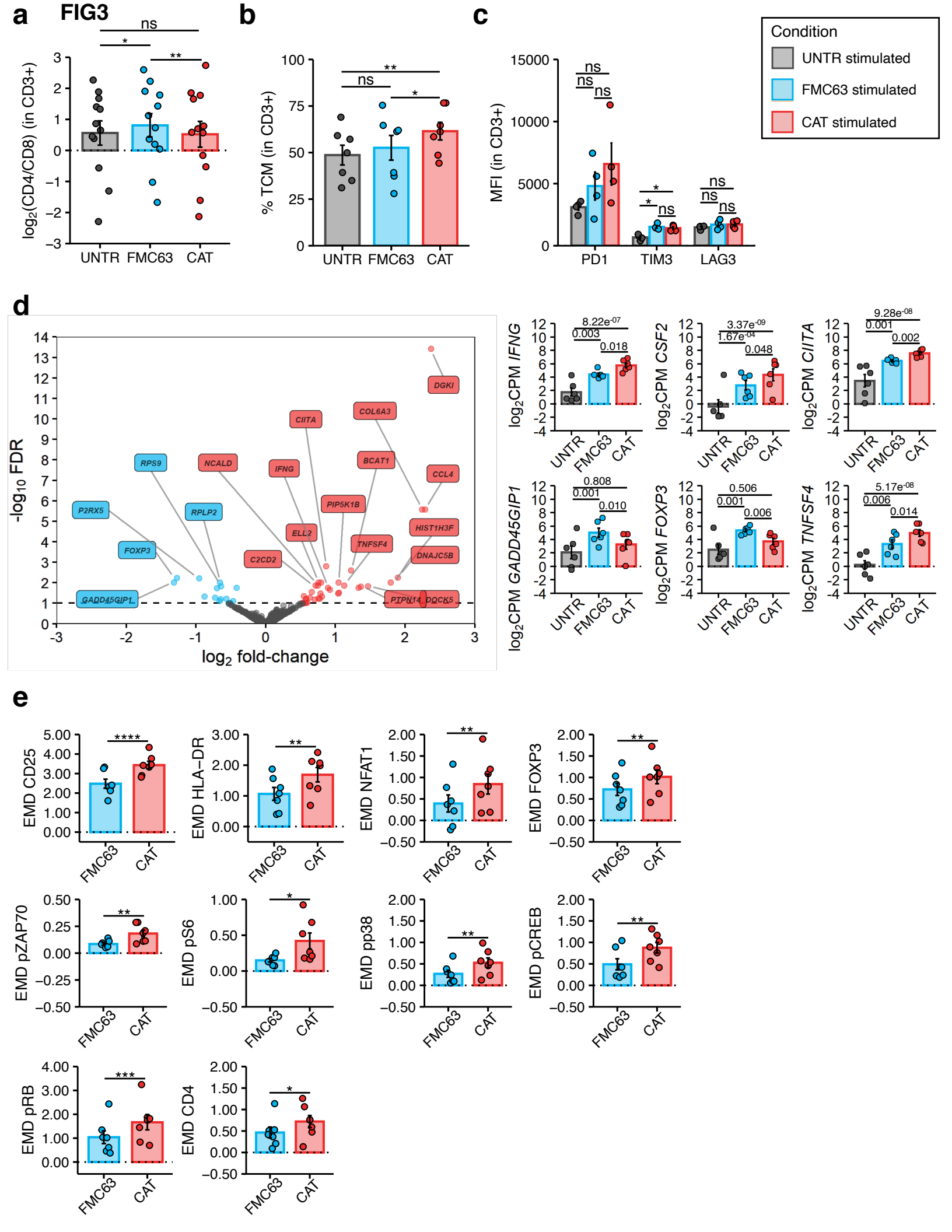
FIG3
a
b
c
d
e
Condition
UNTR stimulated
FMC63 stimulated
CAT stimulated
log2(CD4/CD8) (in CD3+)
% TCM (in CD3+)
MFI (in CD3+)
UNTR
FMC63
CAT
PD1
TIM3
LAG3
-log10 FDR
log2 fold-change
P2RX5
RPS9
NCALD
RPLP2
FOXP3
GADD45GIP1
IFNG
CIITA
ELL2
C2CD2
PIP5K1B
TNFSF4
BCAT1
COL6A3
DGKI
CCL4
HIST1H3F
DNAJC5B
PTPN14
DOCK5
log2CPM IFNG
log2CPM CSF2
log2CPM CIITA
log2CPM GADD45GIP1
log2CPM FOXP3
log2CPM TNFSF4
EMD CD25
EMD HLA-DR
EMD NFAT1
EMD FOXP3
EMD pZAP70
EMD pS6
EMD pp38
EMD pCREB
EMD pRB
EMD CD4

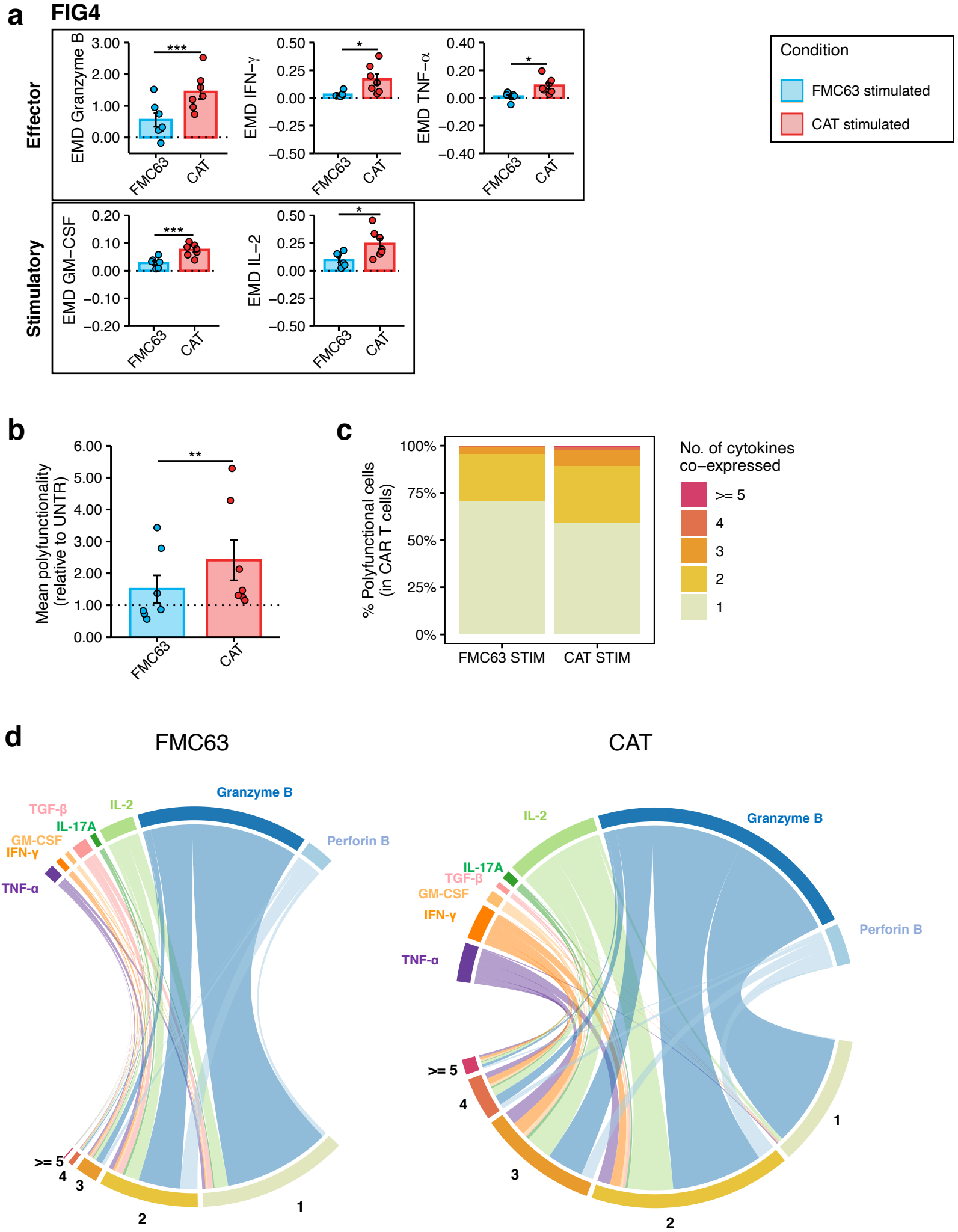
a
FIG4
Effector
EMD Granzyme B
EMD IFN−γ
EMD TNF−α
Stimulatory
EMD GM−CSF
EMD IL−2
FMC63
CAT
Condition
FMC63 stimulated
CAT stimulated
b
Mean polyfunctionality (relative to UNTR)
c
% Polyfunctional cells (in CAR T cells)
FMC63 STIM
CAT STIM
No. of cytokines co−expressed
>= 5
4
3
2
1
d
FMC63
CAT
Granzyme B
Perforin B
IL-2
IL-17A
TGF-β
GM-CSF
IFN-γ
TNF-α

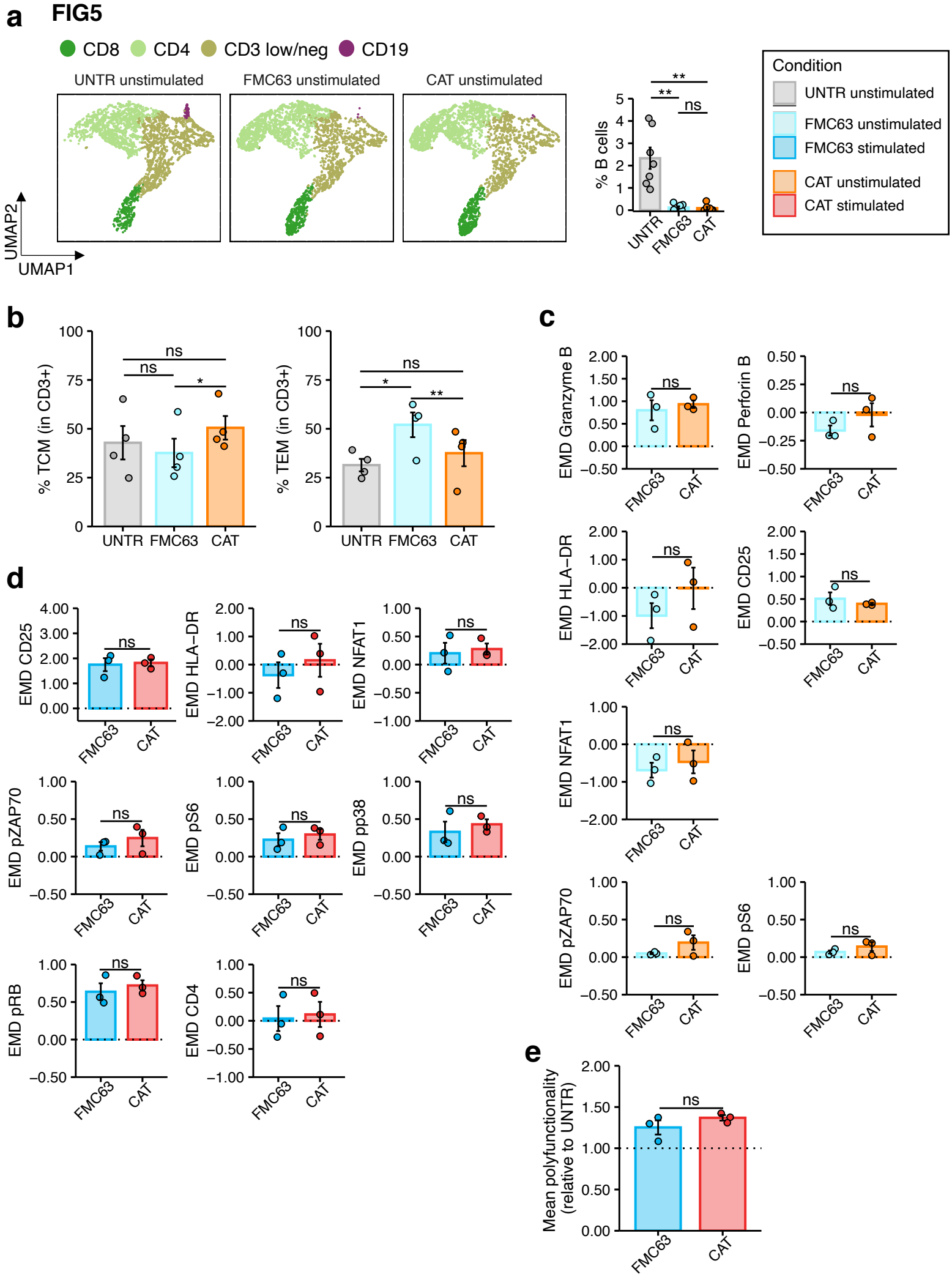
a
FIG5
CD8
CD4
CD3 low/neg
CD19
UNTR unstimulated
FMC63 unstimulated
CAT unstimulated
UMAP2
UMAP1
% B cells
UNTR
FMC63
CAT
ns
Condition
UNTR unstimulated
FMC63 unstimulated
FMC63 stimulated
CAT unstimulated
CAT stimulated
b
% TCM (in CD3+)
% TEM (in CD3+)
c
EMD Granzyme B
EMD Perforin B
EMD HLA–DR
EMD CD25
EMD NFAT1
EMD pZAP70
EMD pS6
d
EMD pp38
EMD pRB
EMD CD4
e
Mean polyfunctionality (relative to UNTR)

SUPPLEMENTARY FIG1

a

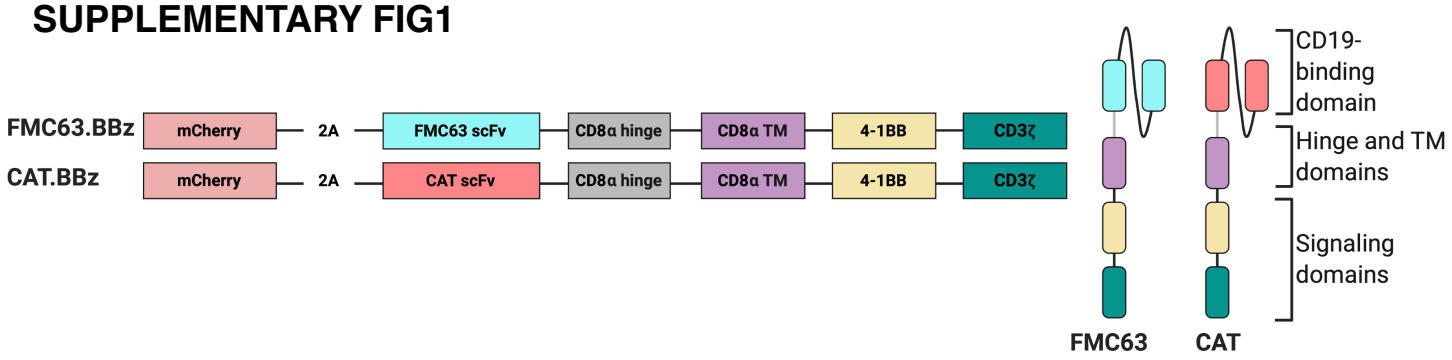

b

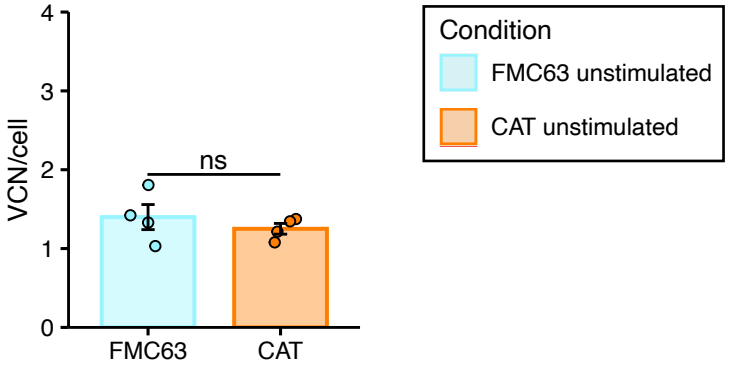

SUPPLEMENTARY FIG2

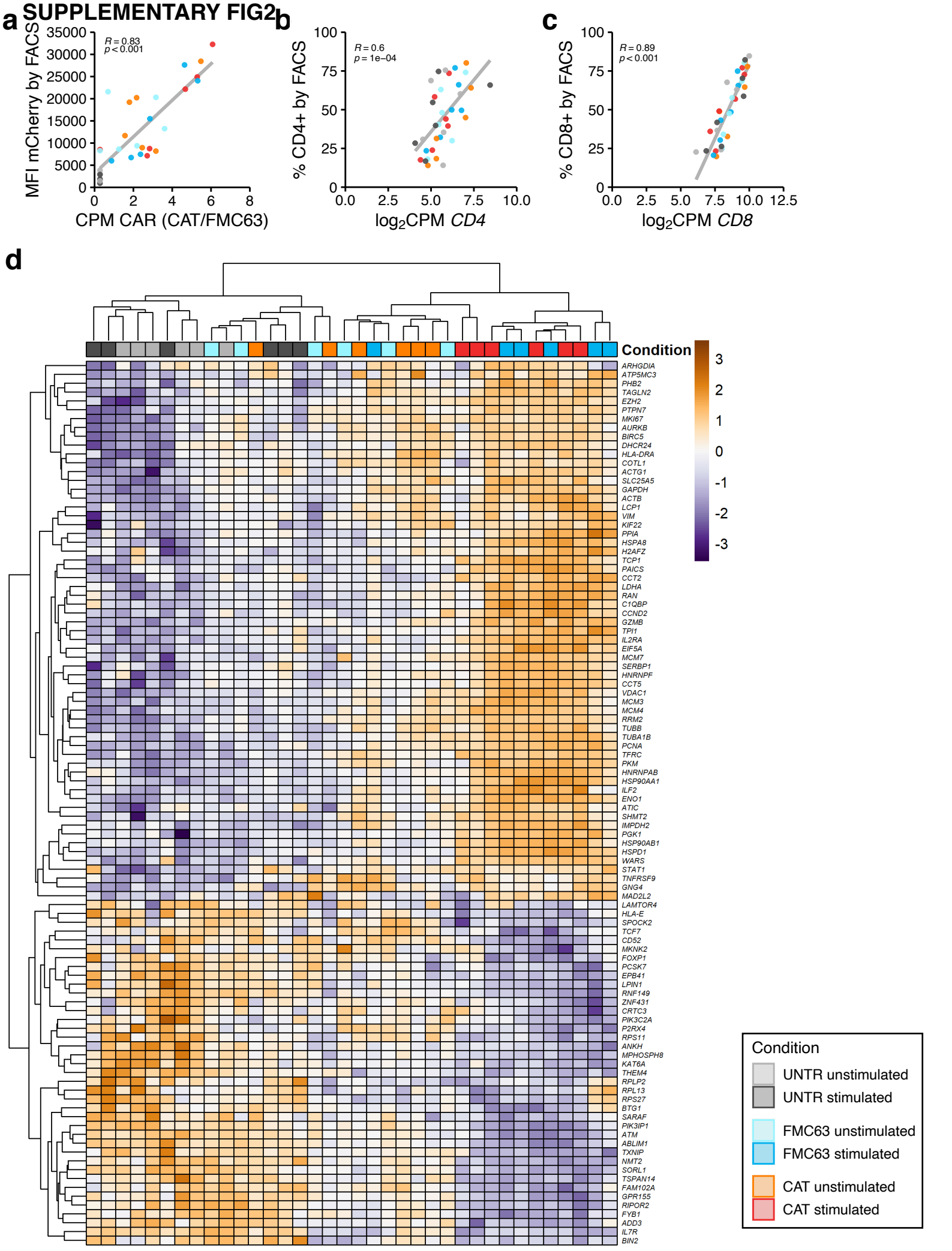

SUPPLEMENTARY FIG3

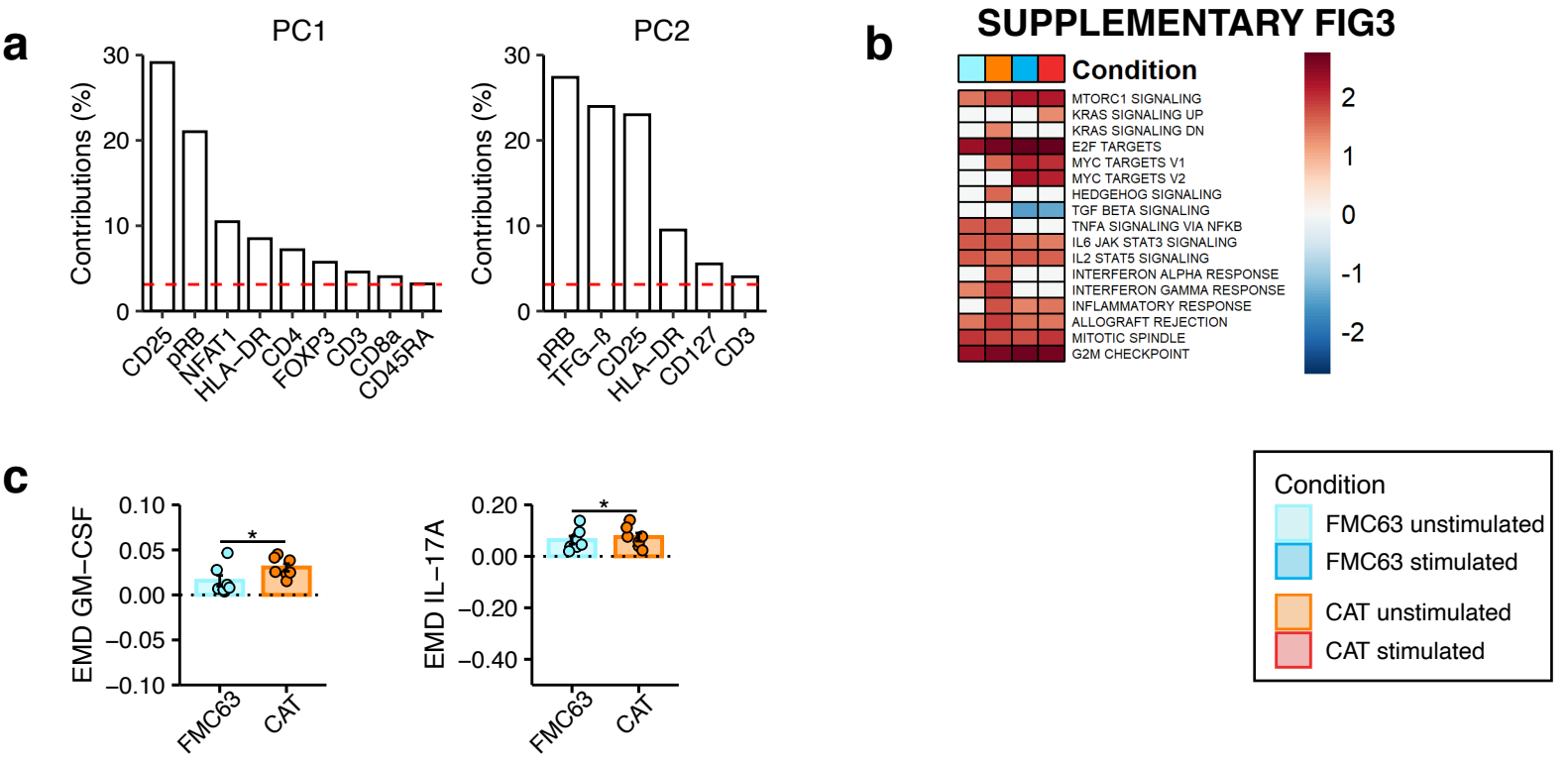

a

SUPPLEMENTARY FIG4

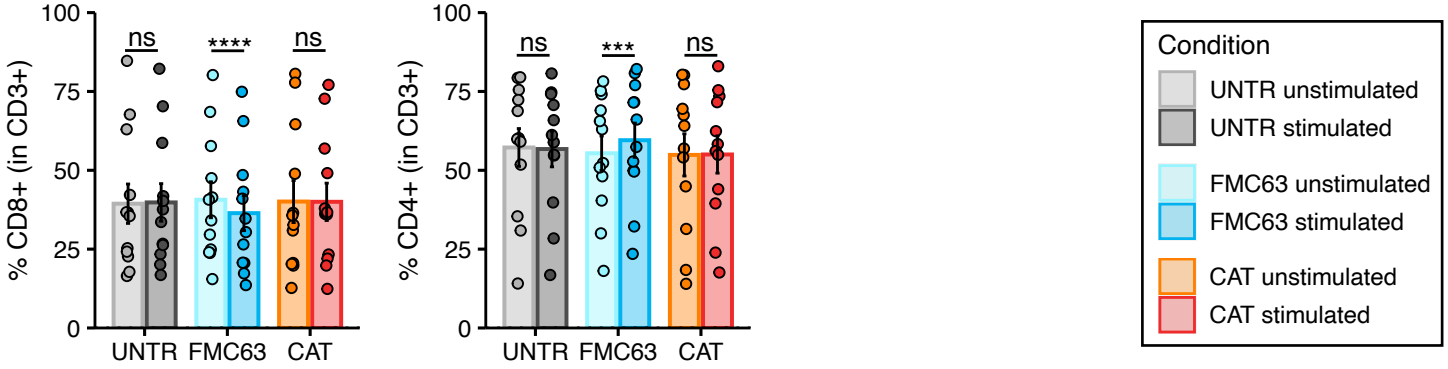

b

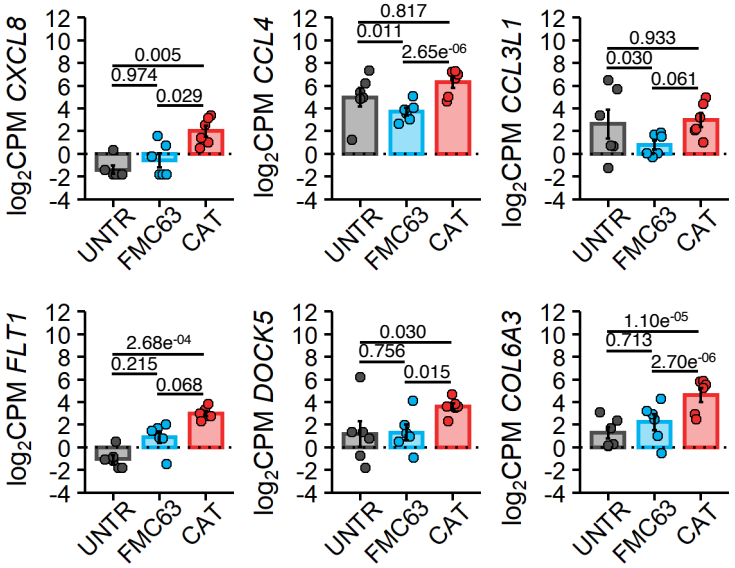

SUPPLEMENTARY FIG5

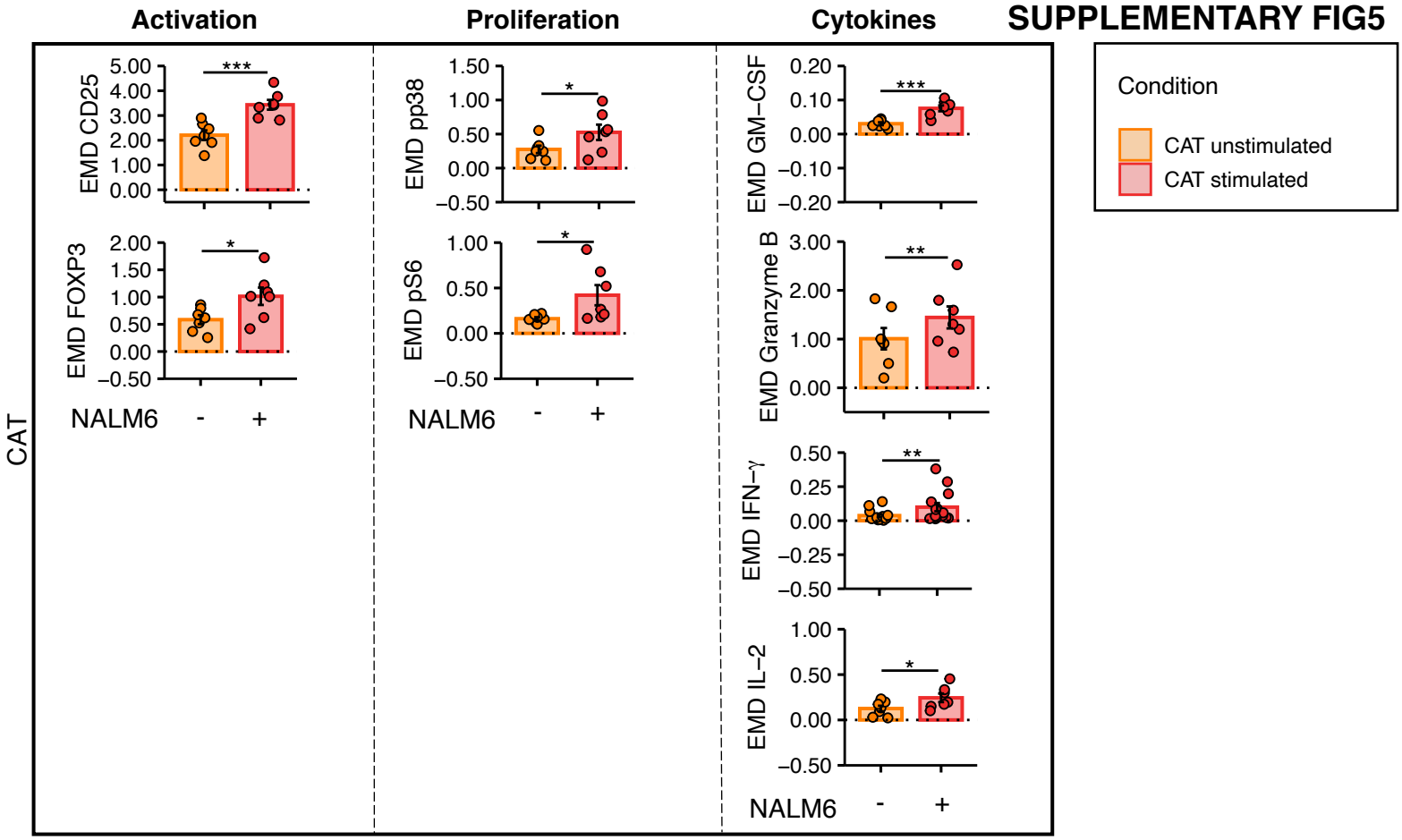

SUPPLEMENTARY FIG6

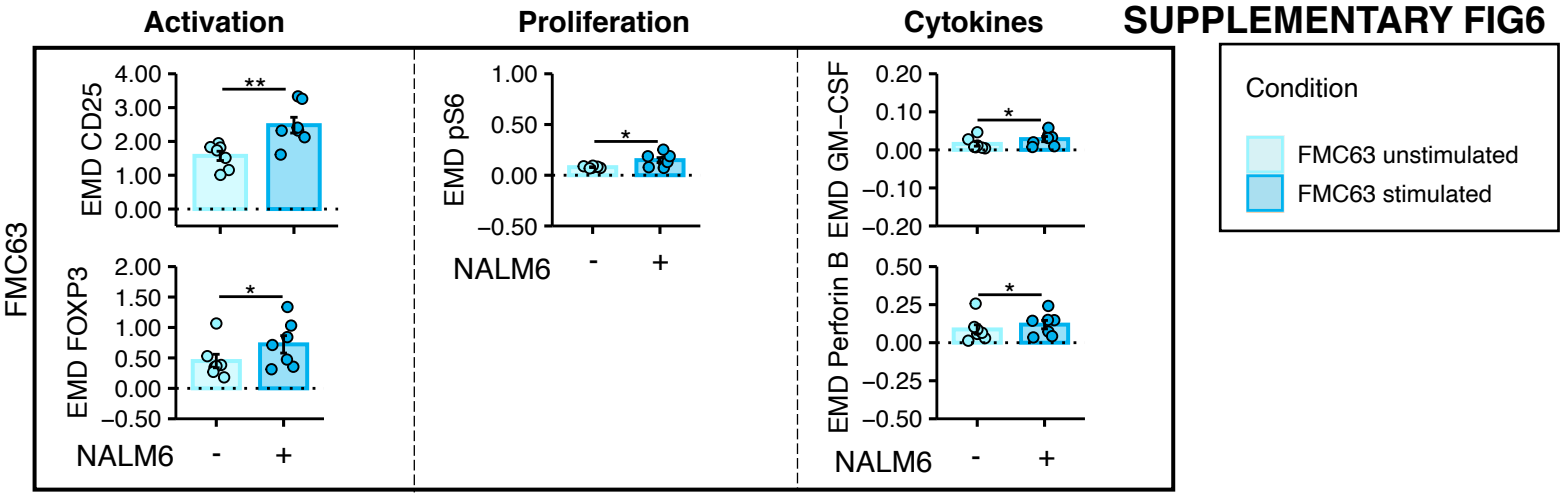

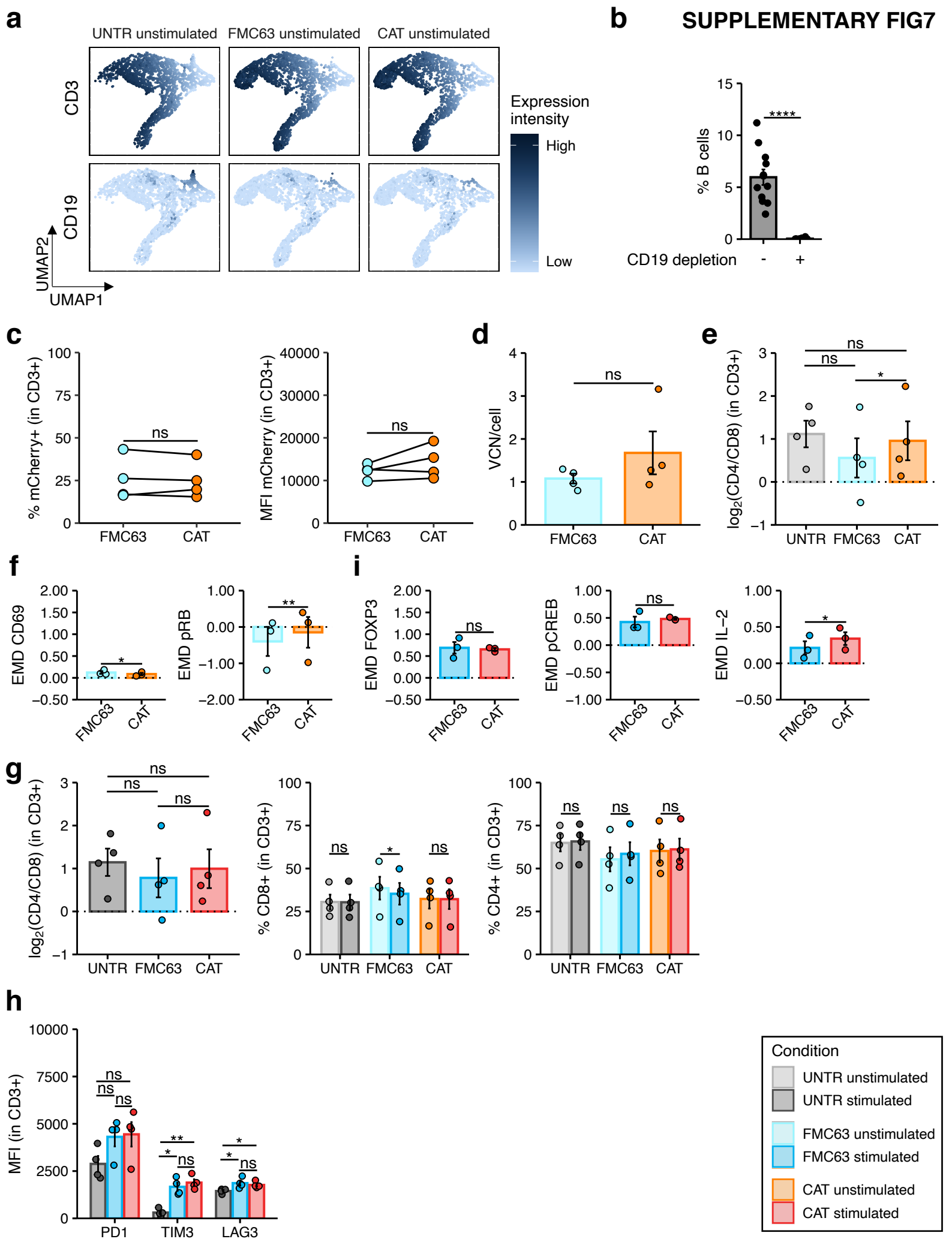
SUPPLEMENTARY FIG7
a
UNTR unstimulated
FMC63 unstimulated
CAT unstimulated
CD3
CD19
UMAP2
UMAP1
Expression intensity
High
Low
b
% B cells
****
CD19 depletion
-
+
c
% mCherry+ (in CD3+)
MFI mCherry (in CD3+)
ns
FMC63
CAT
d
VCN/cell
ns
e
log2(CD4/CD8) (in CD3+)
ns
*
UNTR
f
EMD CD69
EMD pRB
*
**
i
EMD FOXP3
EMD pCREB
EMD IL−2
g
log2(CD4/CD8) (in CD3+)
% CD8+ (in CD3+)
% CD4+ (in CD3+)
h
MFI (in CD3+)
PD1
TIM3
LAG3
Condition
UNTR unstimulated
UNTR stimulated
FMC63 unstimulated
FMC63 stimulated
CAT unstimulated
CAT stimulated

SUPPLEMENTARY FIG8

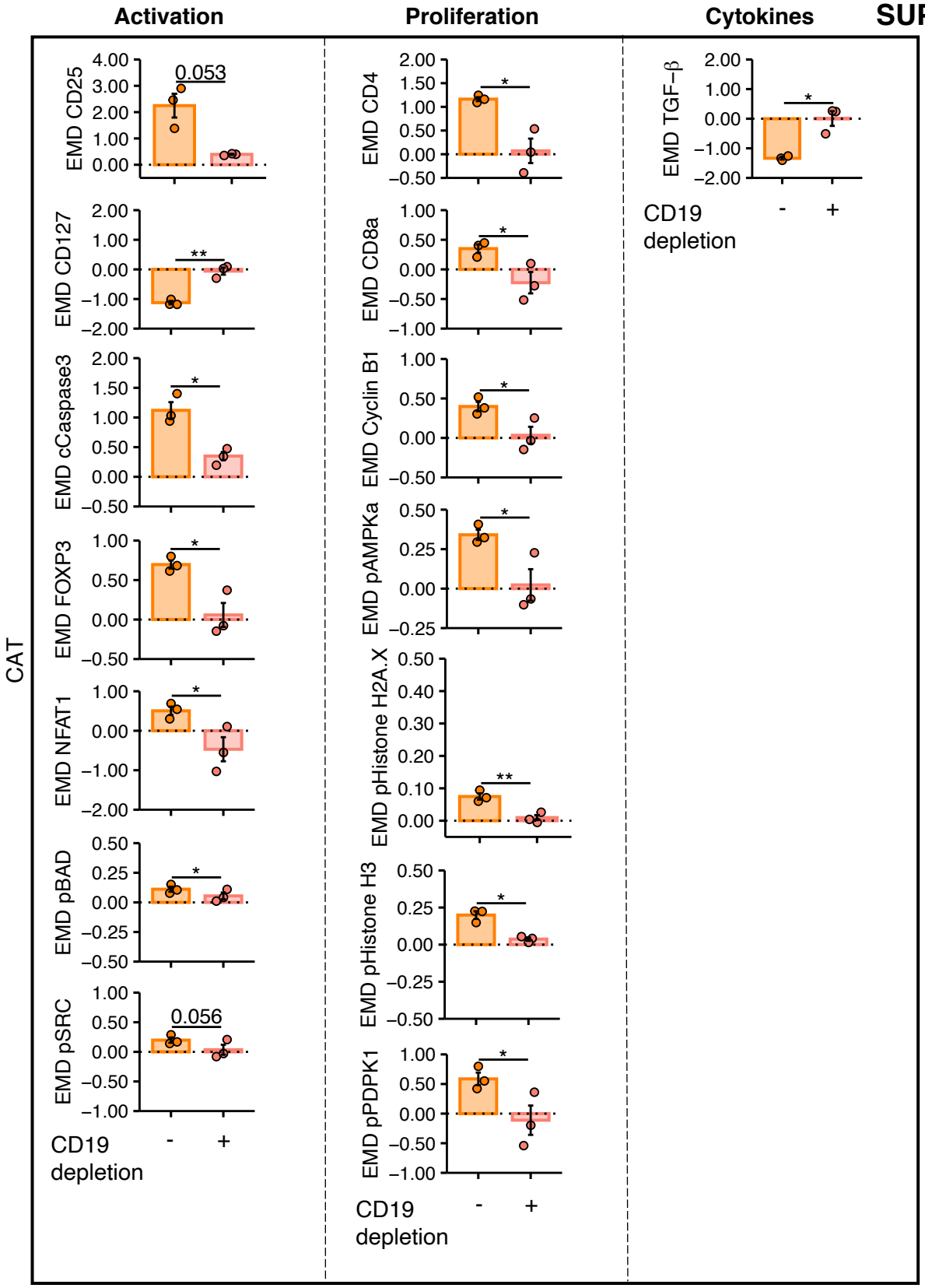

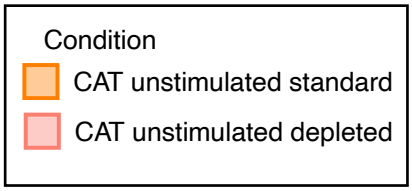

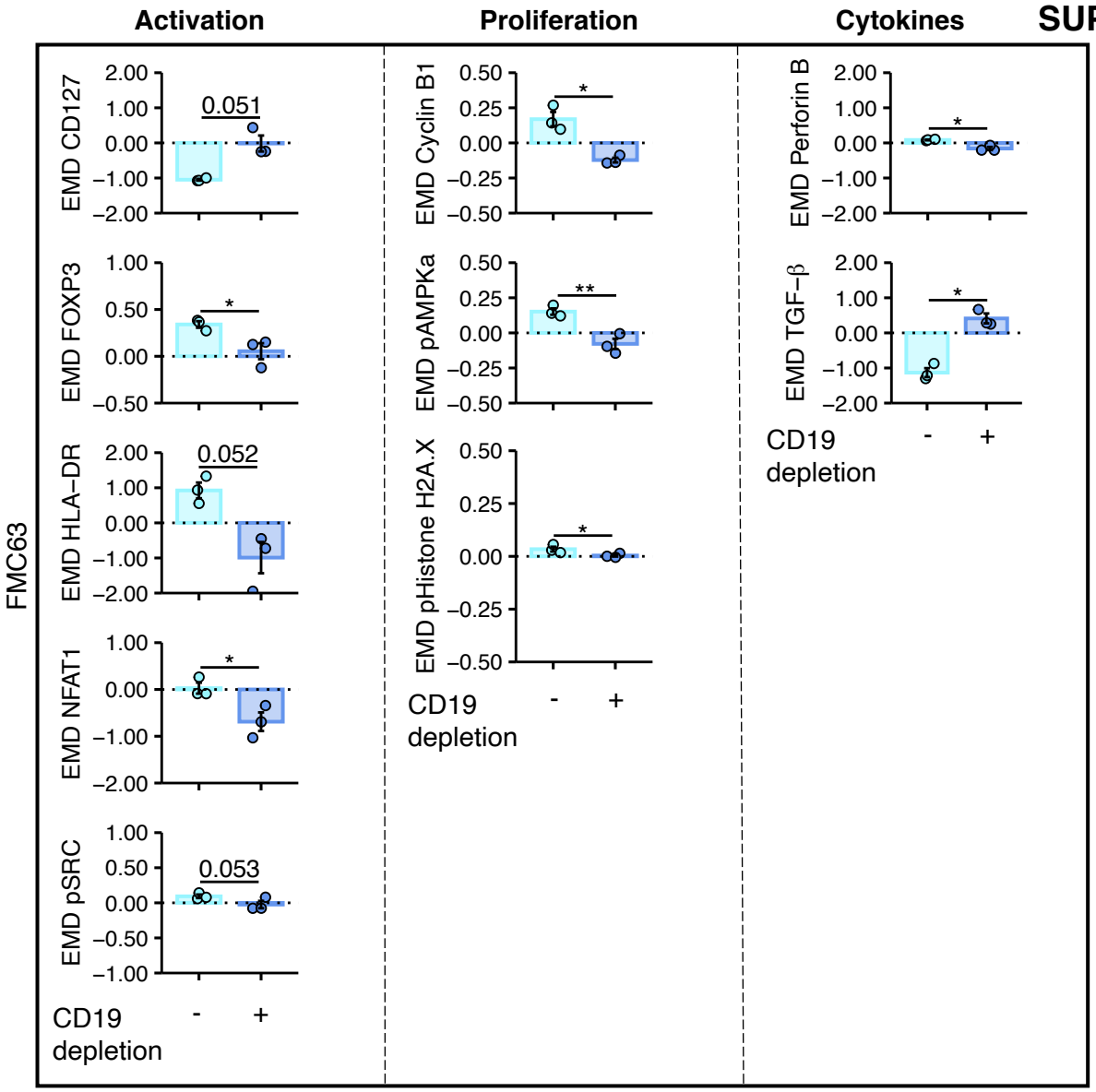
SUPPLEMENTARY FIG9
Activation
Proliferation
Cytokines
FMC63
EMD CD127
0.051
EMD FOXP3
*
EMD HLA−DR
0.052
EMD NFAT1
*
EMD pSRC
0.053
EMD Cyclin B1
*
EMD pAMPKa
**
EMD pHistone H2A.X
*
EMD Perforin B
*
EMD TGF−β
*
CD19 depletion
-
+

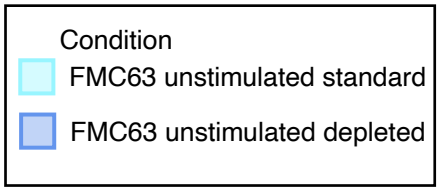
Condition
FMC63 unstimulated standard
FMC63 unstimulated depleted

SUPPLEMENTARY FIG10

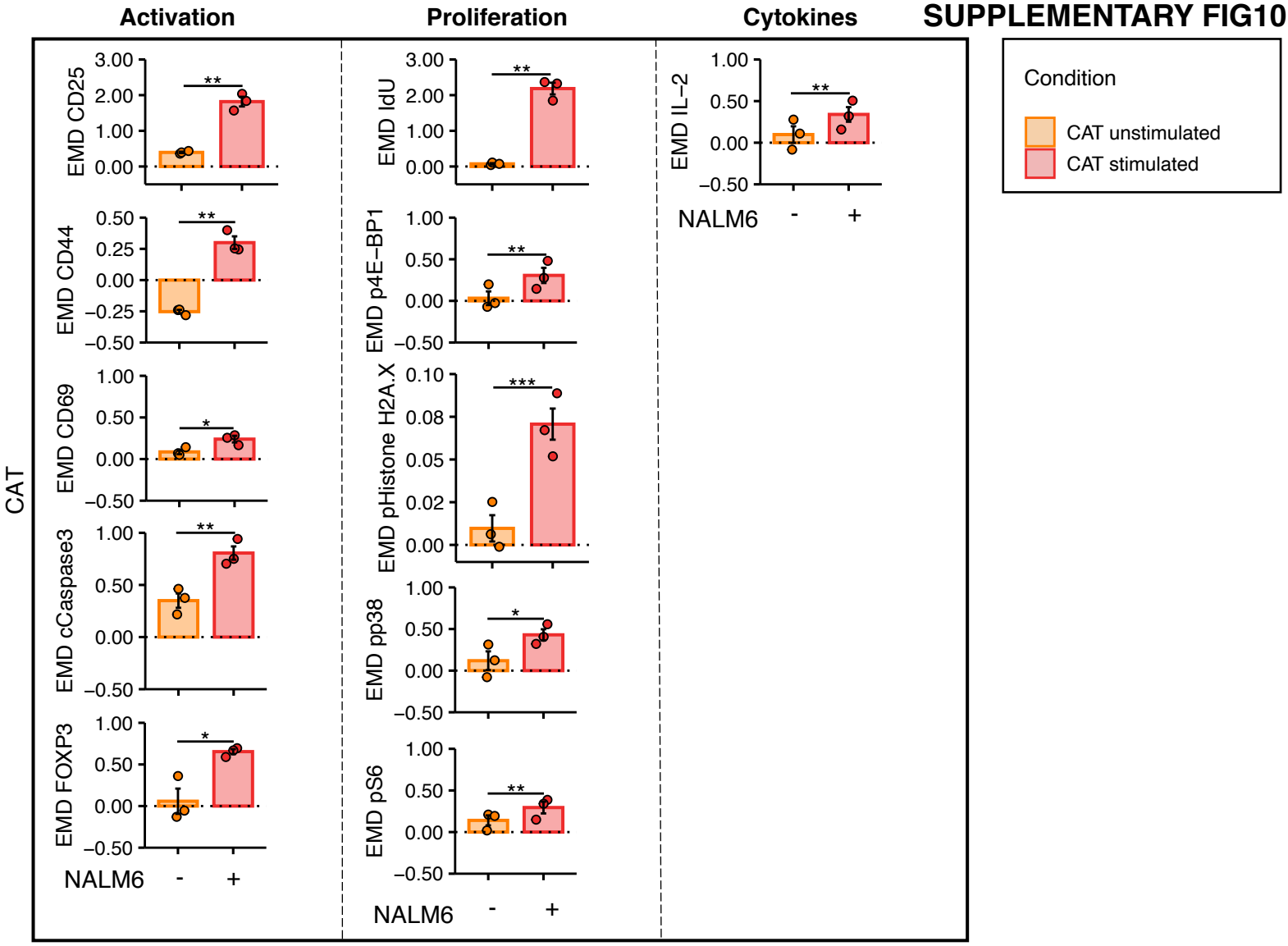
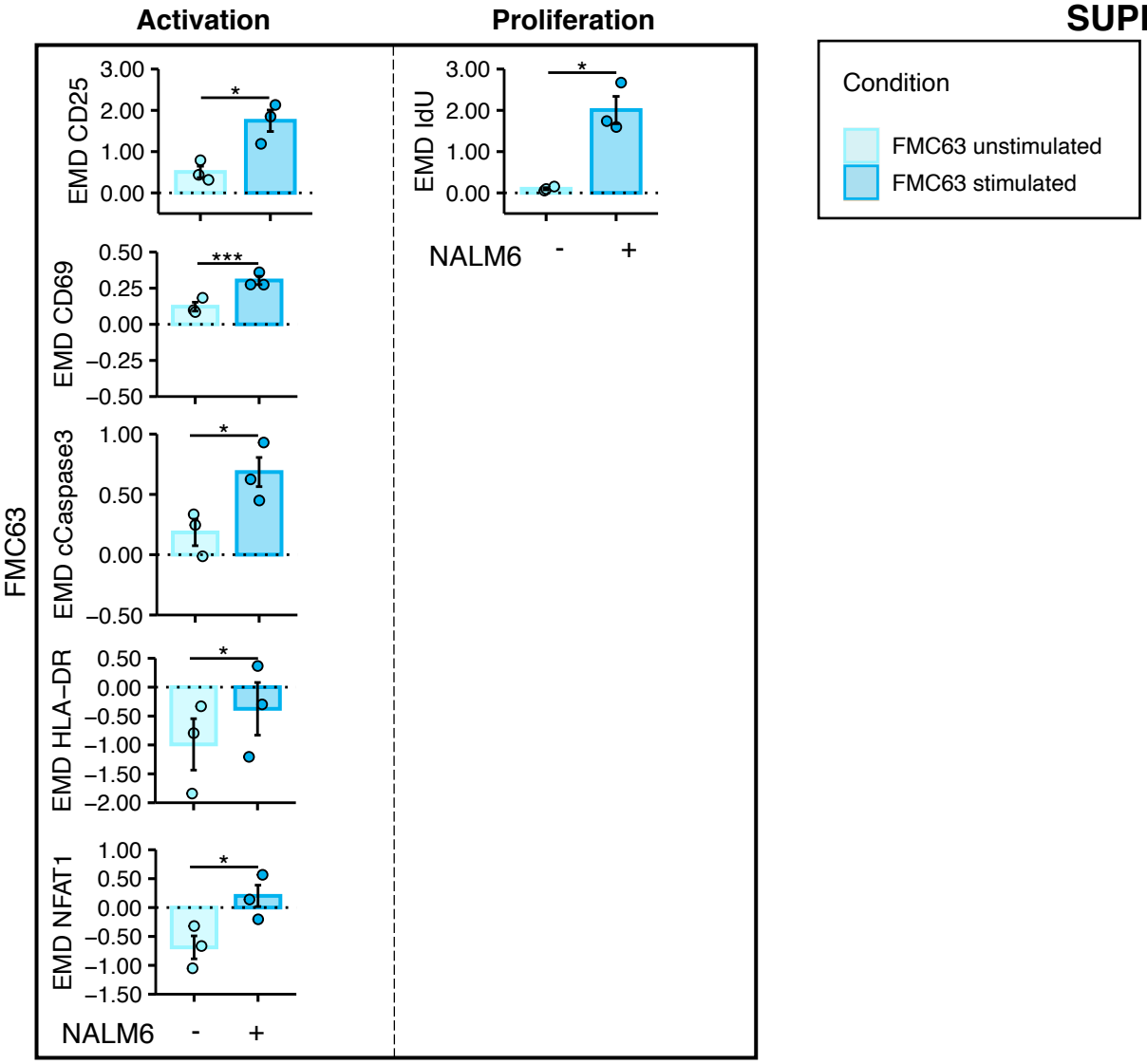
SUPPLEMENTARY FIG11